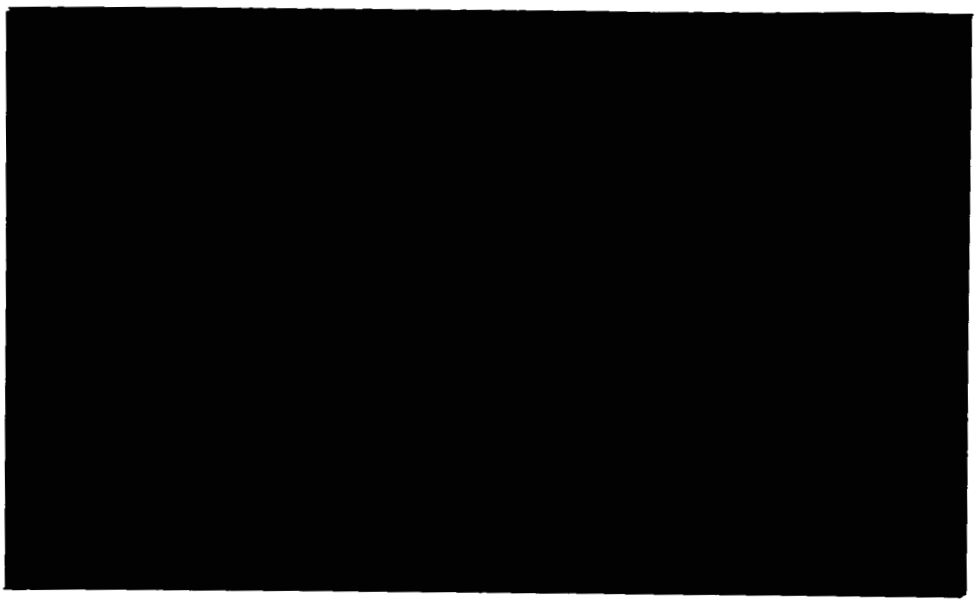

ELECTRO-OPTICAL SYSTEMS, INC.

A Subsidiary of Xerox Corporation

300 N. Halstead Street, Pasadena, California

[redacted]

167

Semiannual Report of Progress

THERMIONIC RESEARCH AND DEVELOPMENT PROGRAM

Prepared for
Jet Propulsion Laboratory
California Institute of Technology
4800 Oak Grove Drive
Pasadena, California

Attention: Mr. Fred Abbott
NASA Procurement Officer

Contract NAS7-514

EOS Report 7118-SA-1 4 February 1967

Prepared by

A. E. Campbell
Program Manager

Approved by

D. G. Worden, Manager
Electron Device Research Section

Approved by

A. O. Jensen, Manager
Electro-Optical Technology Laboratory

ELECTRO-OPTICAL SYSTEMS, INC. — PASADENA, CALIFORNIA
A Subsidiary of Xerox Corporation

CONTENTS

1.	INTRODUCTION	1
2.	ELECTRODE MATERIALS EVALUATION (TASK I)	5
	2.1 Thermionic Emission Microscope	5
	2.2 Vacuum Emission Test Vehicle	11
3.	ELECTRODE MATERIALS EVALUATION (TASK II)	15
	3.1 Interelectrode Spacing at Low Emitter Temperatures (< 2000°K) for the Rhenium-Rhenium/Molybdenum Electrode Systems	17
	3.2 Significance of a Minimum Collector Work Function	29
	3.3 Optimized Converter Performance at Low Emitter Temperatures for the Rhenium-Rhenium Electrode System	34
4.	ANALYSIS AND INTERPRETATION (TASK III)	41
	4.1 Introduction	41
	4.2 Theory of the Vacuum Double Diode	43
	4.2.1 Electron Space Charge in a Double Diode	45
	4.2.2 Poisson's Equation for the Double Diode	51
	4.2.3 Computer Solutions of Poisson's Equation	52
	REFERENCES	57

ILLUSTRATIONS

2-1	Thermionic Electron Emission Microscope, Modification I	6
2-2	Components of Interest in the Thermionic Electron Microscope	8
2-3	Thermionic Emission Microscope Axial Potential Distribution	9
2-4	Lenses, Grid, and Grid Mounting Plate for Thermionic Emission Microscope	10
2-5	Vacuum Emission Vehicle Mounted in Test Fixture	13
3-1	Variable Parameter Test Vehicle	15
3-2	Interelectrode Spacing versus Voltage; Emitter, Collector, and Cesium Reservoir Temperatures Constant	19
3-3	Voltage Output versus Interelectrode Spacing Relationship for T_E = 1627°C, Nonoptimized for Performance Output	21
3-4	Voltage Output versus Interelectrode Spacing for T_E = 1525°C, Nonoptimized Performance	22
3-5	Voltage versus Interelectrode Spacing Relationship for T_E = 1525°C, Optimized for 0.40 Volt Output	23
3-6	Voltage versus Interelectrode Spacing Relationship for T_E = 1525°C, Optimized for 0.5 Volt Output	24
3-7	Voltage versus Interelectrode Spacing Relationship for T_E = 1430°C, Optimized for 0.3 Volt Output	25
3-8	Voltage versus Interelectrode Spacing Relationship for T_E = 1430°C, Optimized for 0.40 Volt Output	26
3-9	Voltage versus Interelectrode Spacing Relationship for T_E = 1330°C, Optimized for 0.20 Volt Output	27
3-10	Comparison Plot of Re-Re System to Re-Mo System Showing Voltage Output Difference of 60 to 80 mW Over Entire Spacing Range	28
3-11	Optimized Performance Plot Comparing Additive Data to EOS Nonadditive Data	32

3-12	Current at 0.5 Volt versus Cesium Reservoir Temperature for T_E = 1527°C	35
3-13	Current at 0.4 Volt versus Cesium Reservoir Temperature at T_E = 1527°C	36
3-14	Current at 0.35 Volt versus Cesium Reservoir Temperature at T_E = 1527°C	37
3-15	Current at 0.4 Volt versus Cesium Reservoir Temperature at T_E = 1427°C	38
3-16	Current at 0.3 Volt versus Cesium Reservoir Temperature at T_E = 1427°C	39
4-1	Typical Voltage Output versus Interelectrode Spacing Curve Showing the Three Characteristics Regions Described in the Text	42
4-2	Schematic Representation of the Electrostatic Potential Energy Due to Electron Space Charge Between Emitter and Collector	44
4-3	Normalized Potential Distribution (η) versus Normalized Coordinate (ξ) in the Interelectrode Space for the Case of α = 2.02215 and Several Values of β	53

SECTION 1

INTRODUCTION

This is the first semiannual report of progress under NASA Contract NAS7-514, an 18-month program to improve the output performance of low temperature thermionic converters (i.e., emitter temperature less than 2000°K) by a systematic investigation of optimized interelectrode spacing and of electrodes yielding a low work function collector. Vapor-deposited rhenium has been selected as the first candidate material, since in a deposit with a preferred orientation of (0001) rhenium should have the highest bare work function of the elemental, metallic surfaces. Those materials possessing a high bare work function have experimentally demonstrated a low work function in the cesium covered condition. To characterize the uniformity of the vapor-deposited rhenium surface, the EOS thermionic emission microscope has been modified to operate at higher temperatures and magnifications. In addition to surveying the surface uniformity, the microscope is being modified to include measurement of the work function of individually selected grains. To supplement the microscope study, a vacuum emission vehicle of guard-ringed design will be utilized to measure the average bare work function of selected surfaces. From the results obtained on these two devices, vapor-deposited rhenium emitters which demonstrate the highest bare work function, and the highest degree of preferred orientation and surface uniformity will be selected for further evaluation in a variable parameter test vehicle.

The test vehicle evaluation will consist mainly of three areas of investigation. The first will be the measurement of a minimum cesiated work function. Second, the voltage output versus interelectrode spacing will be measured and compared to the recently acquired data from

polycrystalline rhenium. Finally, the test vehicle will be instrumented and tested as a thermionic converter for optimized performance, particularly in the low emitter temperature region. The results from these three sets of measurements will in turn be applied to the design, fabrication, and test of high performance low temperature cylindrical converters.

The work accomplished to date on this program is summarized briefly:

a. The EOS variable parameter test vehicle has been demonstrated to be sufficiently versatile to operate at wide spacings and low emitter temperatures without extensive redesign.

b. Reproducible data from converter hardware and test vehicles have substantiated the hypothesis that a higher bare work function material yields a lower cesiated work function. And, of equal importance, a lower collector work function yields correspondingly higher power output. This increased power output in the case of low temperature thermionic converters can exceed 30 percent of presently available power density output achieved with the more usual cesiated molybdenum collectors.

c. The pressure-distance or "pd" product of 16.0 ± 0.8 mil-torr is independent of emitter temperature or collector material.

d. Two ultra high vacuum devices have been designed and fabricated for the purpose of characterizing and assessing the quality of vapor-deposited rhenium surfaces prior to committing them as electrodes in a thermionic converter. Essentially two types of measurements will evolve from these devices: qualitative thermionic emission images of the electrode surface which will indicate the degree of surface uniformity, and quantitative measurements of the electrode work function.

A separate task devoted to the theoretical analysis of the experimental data supplements these experimental investigations. During this report period the analytic effort has been devoted to examination of the very close spaced cesium thermionic converter which operates in the space charge mode with dual emitting electrodes. This analysis is being

extended to larger spacings to describe a thermionic converter operating in the preignition mode. Subsequent effort will be devoted to the region of onset ionization, positive column formation, and the collector sheath.

SECTION 2

ELECTRODE MATERIALS EVALUATION (TASK I)

Two special-purpose devices are being assembled to evaluate candidate electrode materials. The first device, a vacuum emission vehicle, has been designed and built to measure the average bare work function (effective) for selected emitters of vapor-deposited rhenium. The second device, the EOS thermionic emission microscope, has been modified to include a special lens and high voltage section to examine the fine grain structure of vapor-deposited rhenium. In addition, a Faraday cup will be incorporated into the emission microscope for the purpose of measuring the work function (effective) of individual grains. For a large number of grains, the average value of these individual measurements will provide a comparison to the average measurement from the vacuum emission vehicle.

The design of these devices allows for transfer of the entire emitter subassembly from one vehicle to the other. Therefore, characteristics of a selected emitter surface will be measured and observed in both devices before being committed to a variable parameter test vehicle.

The major effort on this task has been in the design and fabrication of the two vehicles. The following subsections describe the design goals, special fabrication considerations and operational features of both devices.

2.1 THERMIONIC EMISSION MICROSCOPE

Figure 2-1 is an assembly drawing of the modified microscope indicating the location of the Faraday cup and high magnification lenses. In its

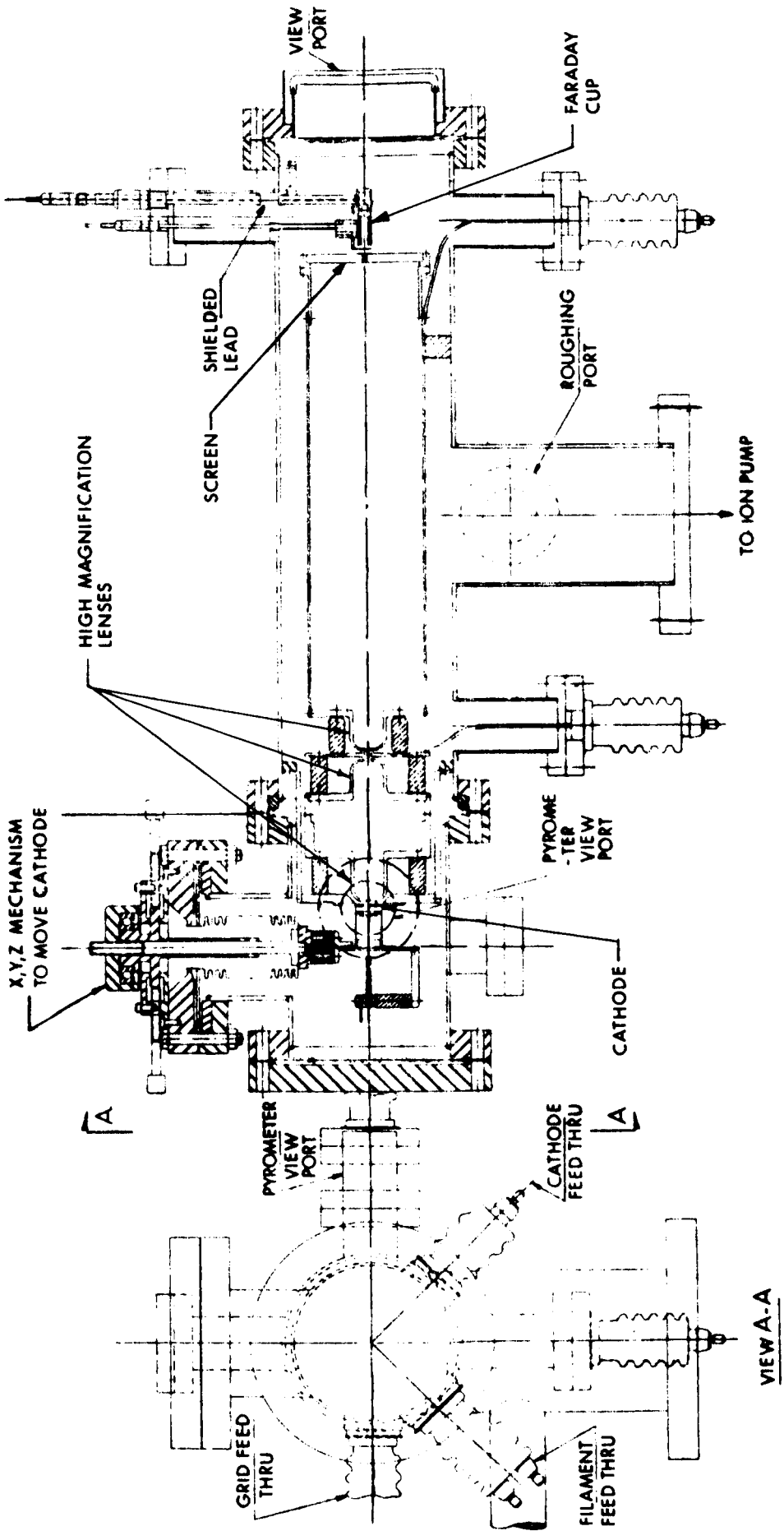

FIG. 2-1 THERMIONIC ELECTRON EMISSION MICROSCOPE, MODIFICATION I

completed form, the emission microscope will be capable of 1000X magnification, 0.1 micron resolution, and cathode temperatures of 2000°K in a vac-ion pumped environment of 10^{-8} to 10^{-9} torr background pressure. Figure 2-2 is a photograph of the thermionic emission microscope structure with the various components of interest identified. The structural material is stainless steel type 304 flanged together with Varian-type fittings and mounted with high voltage Alite insulators to permit complete bake-out before operation. The microscope, as assembled on a 140 l/sec vac-ion pump, has been checked for stray magnetic field intensity. The presence of a 2 or 3-gauss magnetic field could disturb the electron beam trajectory and result in poor quality images on the screen. A gauss meter (R.F. Lab, Inc.) measurement in the microscope interior shows a 0.15 to 0.25-gauss field which is essentially the Earth's magnetic field.

Figure 2-3 describes the axial potential distribution of the modified lens system. The cathode is heated indirectly by electron bombardment. In turn, the thermionically emitted electrons are drawn through the grid and accelerated into the screen section. The aluminized screen was purchased from the Video Color Corporation as a nonbrowning phosphor screen which will withstand 30 kilovolt electron bombardment. As indicated in the figure, a beam decelerating collector is used in conjunction with the Faraday cup.

Figure 2-4 is a photograph of the high temperature tantalum grid, the copper grid mounting plate, and two of the stainless steel lenses. All corners and cutouts in these parts are fully contoured to reduce high local fields and the accompanying possibility of field emission. The lenses contain a central aperture which is nominally 0.080 inch diameter with a ±0.002 inch tolerance. However, the ellipticity of the hole is critical to the focusing action of the lens, and a roundness tolerance of 0.0004 inch is required for minimum aberration of

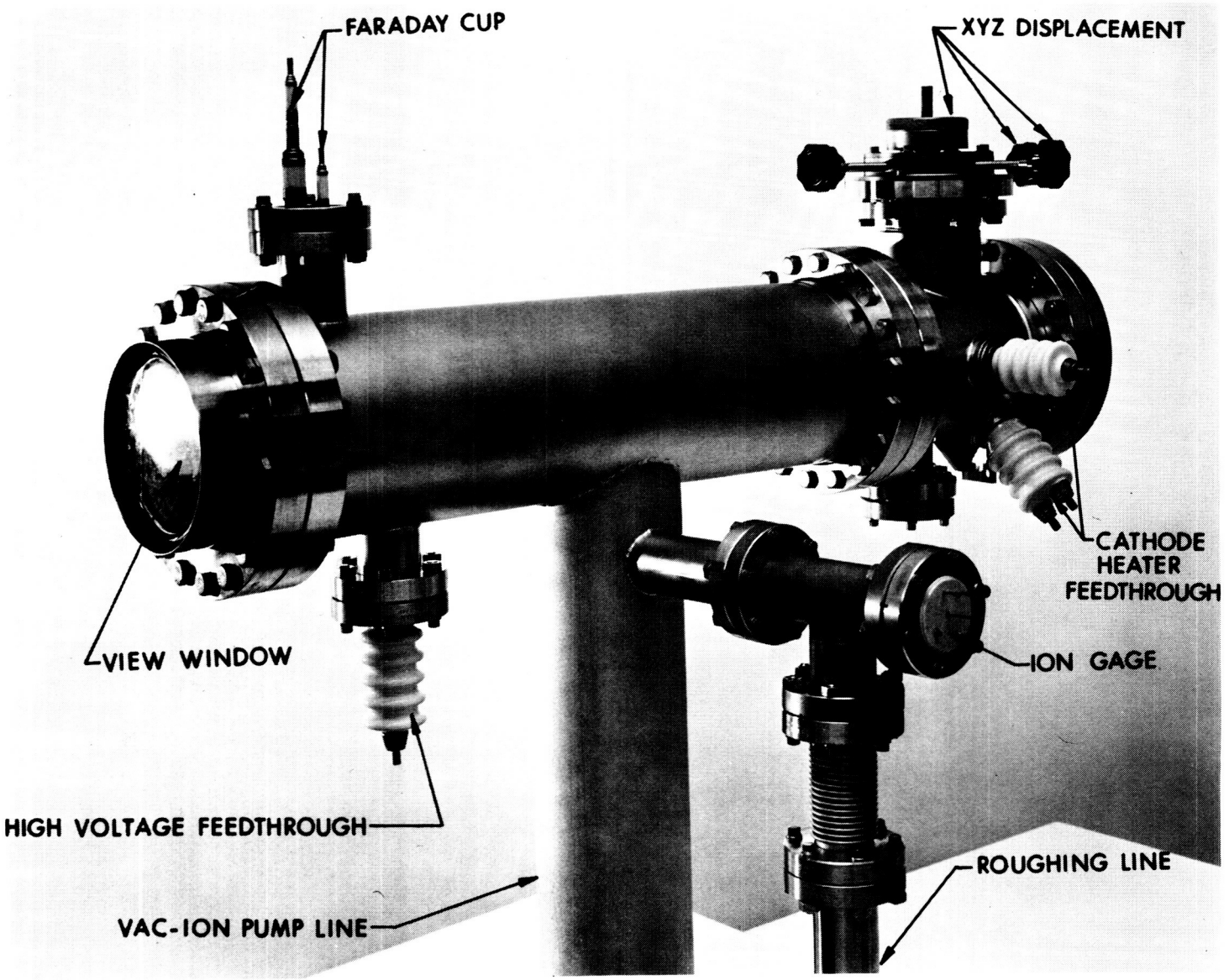

FIG. 2-2 COMPONENTS OF INTEREST IN THERMIONIC ELECTRON MICROSCOPE

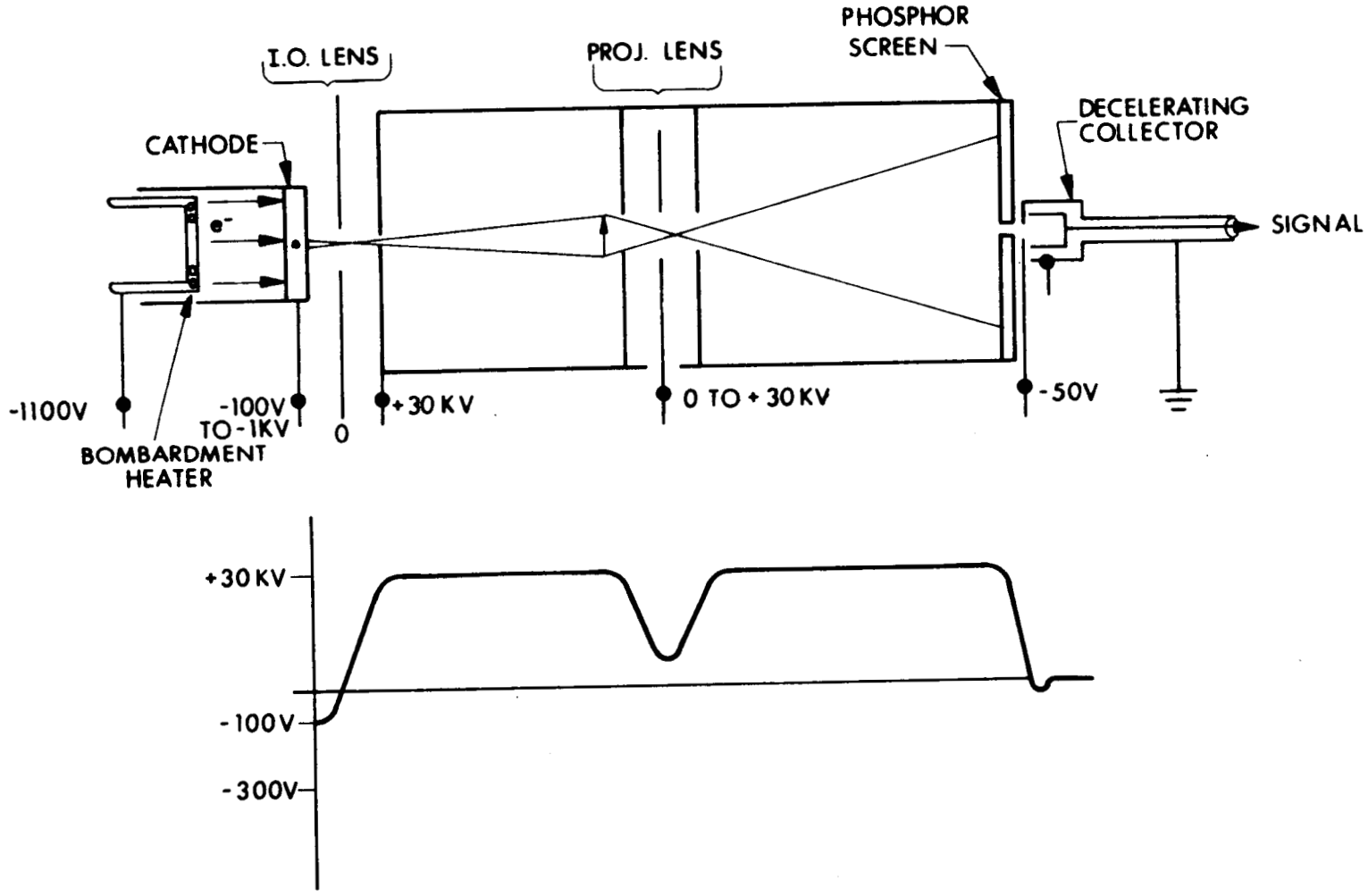

FIG. 2-3 THERMIONIC EMISSION MICROSCOPE AXIAL POTENTIAL DISTRIBUTION

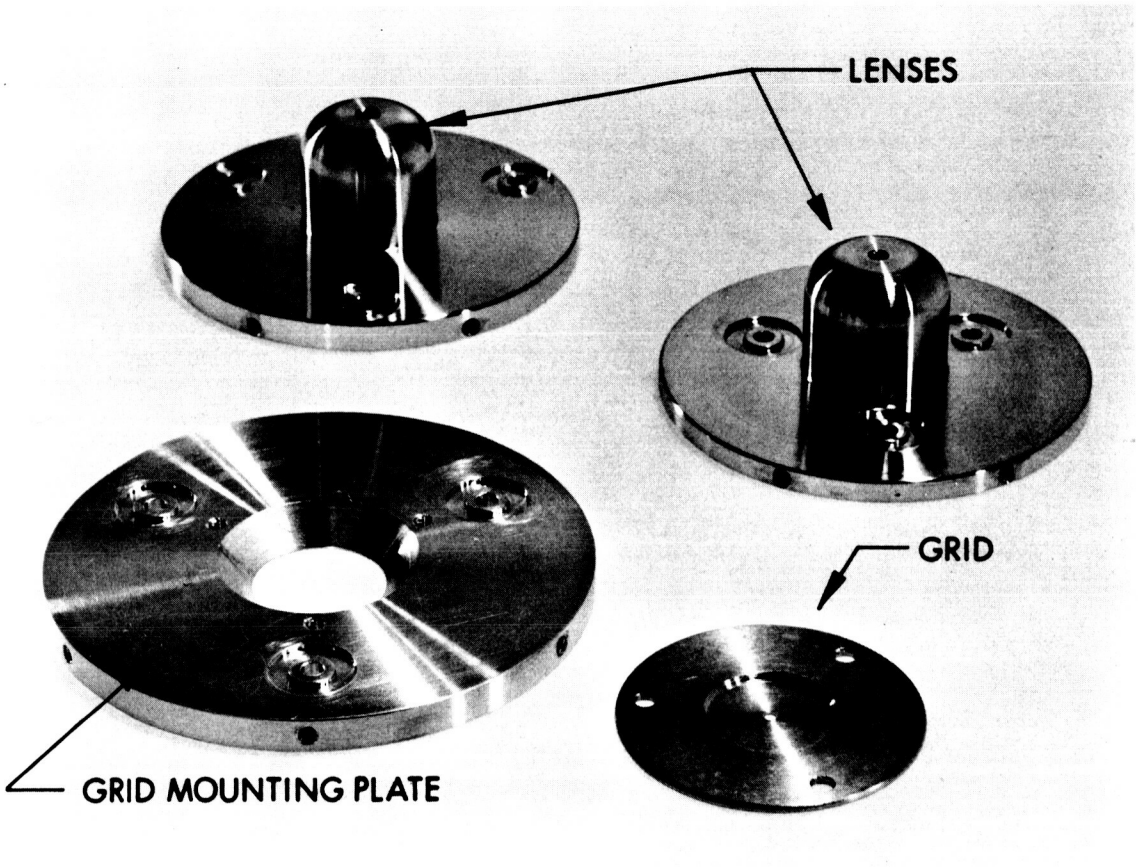

FIG. 2-4 LENSES, GRID, AND GRID MOUNTING PLATE FOR THERMIONIC EMISSION MICROSCOPE

the beam. A precision gauge company will provide the finish honing, inspection, and certification of these apertures.

2.2 VACUUM EMISSION TEST VEHICLE

The second phase in the characterization and evaluation of vapor-deposited rhenium electrode surfaces will consist of measurements of their vacuum thermionic electron emission. These measurements will be performed in a guard ring, planar emission vehicle under ultrahigh vacuum conditions. The specific purpose of these measurements will be to obtain the average Richardson and effective work function via Schottky plots.

The vacuum emission vehicle has three major components: emitter sample stage, guard ring, and collector. The sample stage is designed to accommodate the same emitters used in the thermionic emission microscope and will have provisions for heating the sample by electron bombardment to over 2100°C. Sample temperatures will be measured by a calibrated optical pyrometer focused in a 10:1 hohlraum located in the side of the sample and parallel to the emitting surface. The sample stage will be operated at a below-ground potential during the emission measurements.

The collector electrode is mounted parallel to the sample at a spacing of 40 mils or less, and will intercept the electron emission from the central 2 cm^2 of the emitter surface. Due to the anticipated high work function of vapor deposited rhenium, the electron emission may not exceed more than a few milliamperes at the highest temperature. Consequently, the applied potential required for saturation will be of the order of 10 volts. However, to define the Schottky line, it is expected that the applied voltage may approach two kilovolts. It is anticipated that the Schottky enhancement of the saturated current at a spacing of 40 mils will be only about 20 percent.

The collector is heated directly by radiation from the sample and by emission electrons dissipating energy gained from the applied field between emitter and collector. At the highest voltage and current levels, this amounts to over 50 watts which will be rejected thermally. The present design of the collector structure includes a radiation fin with approximately 80 cm^2 coated with Rokide "C". This radiating area will adequately control the thermal balance of the collector and allow it to operate at temperatures less than 500°C.

The guard ring is spaced concentric to, and about 5 mils from, the collector as indicated in Fig. 2-5. It covers the area of the sample not covered by the collector. The guard ring also will be provided with a radiator fin which will operate at about 500°C.

The electron emission currents to the guard ring and collector will be metered independently. The electrical leads to these components will be operating at potentials within a fraction of a volt of the ground potential. This type of operation minimizes the possibilities for systematic current measuring errors due to leakage. To further minimize leakage currents across the mounting insulators, a null circuit has been devised which guards the collector current leads.

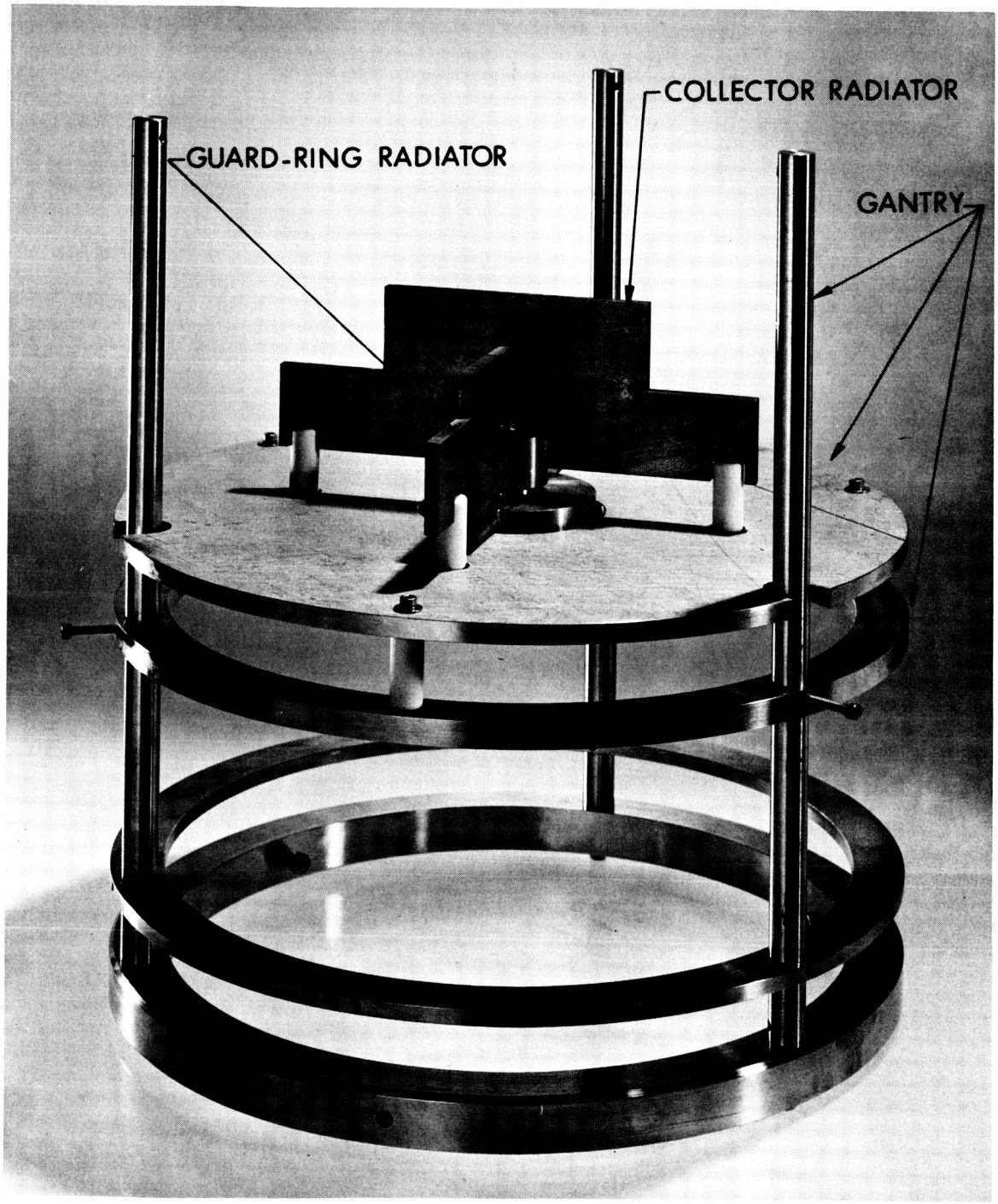

FIG. 2-5 VACUUM EMISSION VEHICLE MOUNTED IN TEST FIXTURE

SECTION 3

ELECTRODE MATERIALS EVALUATION (TASK II)

As a starting point for this investigation, a variable parameter test vehicle previously built and tested by EOS for high temperature thermionic performance was operated at lower emitter temperatures (i.e., from 1327°C to 1735°C true hohlraum) to establish the test vehicle usefulness outside the range of the original design goals. This test vehicle which was designed to operate at 200 to 400 amperes, steady-state, and interelectrode spacings varying from 0.0001 to 0.015 inch has been described elsewhere (Ref. 1, 2).

Figure 3-1 displays the relatively massive structure of the test vehicle necessary to accommodate the high current loads. In the absence of such current loads, the possibility existed that the collector might not operate at a high enough temperature to permit full optimization. Moreover, even if the collector temperature could be optimized, it was possible that some portion of the vehicle proper such as the seals or guard ring structure would operate at a temperature near or below the cesium reservoir temperature and preclude control of the cesium vapor pressure. Finally, and perhaps most critically, the question remained whether or not the single-convolute niobium bellows was capable of 0.020-inch excursions, a spacing arbitrarily selected which would enable power output optimization at emitter temperatures as low as 1250°C.

From the data presented in the following paragraphs, it has been well established that the original design of the test vehicle accommodates an adequate range of variation in thermionic parameters for the purpose of this investigation. Summarized, the range of operation from these test vehicles has been:

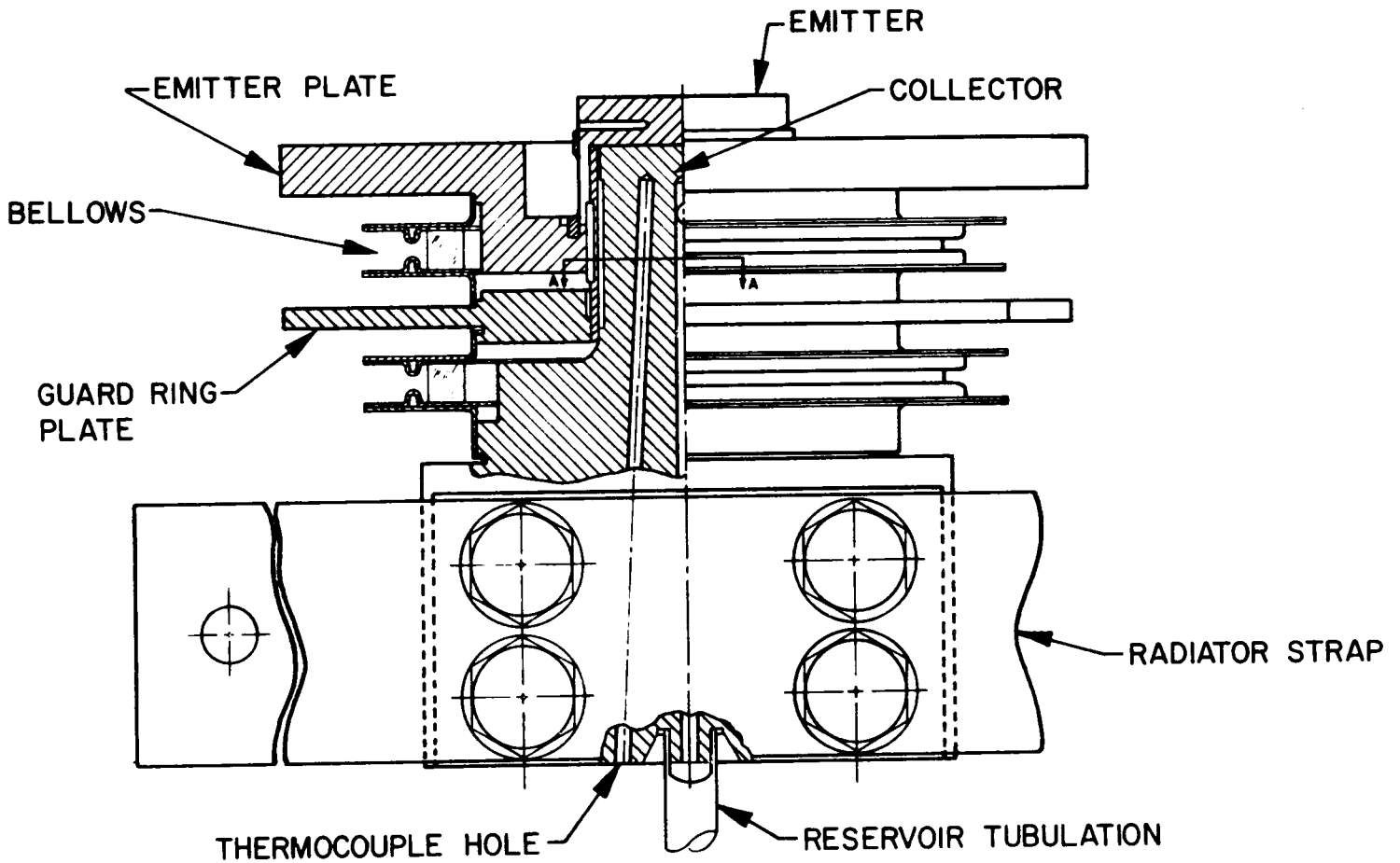

FIG. 3-1 VARIABLE PARAMETER TEST VEHICLE

$T_{emitter}$	-	1735°C to 1327°C true hohlraum (although the emitter was operated in excess of 2150°C during rhenium evaporation processing of the collector)
$T_{collector}$	-	480°C to 1000°C
Spacing	-	< 0.0001 to 0.026 inch
T_{cesium}	-	127°C to 503°C
$J_{current}$	-	2 A/cm^2 to 180 A/cm^2

The initial design of the EOS variable parameter test vehicle has thus provided the present program with a high-precision, high-reliability design for characterizing the low emitter temperature (i.e.,< 2000°K) region of converter operation.

3.1 INTERELECTRODE SPACING AT LOW EMITTER TEMPERATURES (< 2000°K) FOR THE RHENIUM-RHENIUM/MOLYBDENUM ELECTRODE SYSTEMS

It was previously noted that the characterization of this electrode system at higher emitter temperatures had been completed. The electrode system of rhenium-molybdenum has been determined to be unstable. That is, high temperature operation of the emitter provides a sufficient amount of evaporated rhenium on the collector surface to change the work function from a cesium-on-molybdenum system to a cesium-on-rhenium system. Subsequent long term,low temperature operation of the device resulted in the diffusion of the evaporated rhenium into the molybdenum collector substrate resulting in a final collector system consisting of cesium-on-molybdenum. The quantitative difference between these electrode systems is 0.080 volt, as measured in the test vehicle and reproduced independently in a fixed-spacing converter of rhenium-molybdenum electrodes.

To maintain a stable system of rhenium-rhenium electrodes in the presence of diffusion, the rhenium emitter was periodically operated

at temperatures as high as 2200°C for 3 hours (with the cesium reservoir heater turned off) to insure at least a two or three monolayer coverage of rhenium on the collector surface.

The data from a previously examined rhenium-rhenium system compares within 1 or 2 percent of the rhenium-evaporated rhenium-on-molybdenum system (Ref. 3). Hence the low temperature data reported for the rhenium-rhenium/molybdenum system is to be considered, within the experimental error, a rhenium-rhenium system.

Perhaps the most useful data from a variable parameter test vehicle is the voltage output versus interelectrode spacing for constant currents, constant emitter temperature, constant collector temperature, and constant cesium vapor pressure. For if these element temperatures are truly maintained constant and the spacing between electrodes precisely determined, some important phenomenological information as well as engineering optimization data is present in one display. Figure 3-2 is a typical representation of voltage output versus interelectrode spacing for a high temperature case of $T_{emitter}$ = 1735°C. From this figure, the region of extremely close-spaced electrodes may be identified as resembling an electron space-charge type of operation wherein the voltage output drastically increased with decreasing spacing. Secondly, a region of onset of ionization is observed, which leads to an optimum spacing for maximum power output at maximum output voltage. Finally, a region of the characteristic is observed wherein the voltage output decreases more or less linearly with increasing spacing indicative of a positive column in the more usual gas discharges.

At lower emitter temperatures and over a wide range of cesium reservoir temperatures, the same general phenomenon is observed with the pressure-distance product, "pd", at the point of optimum voltage output remaining

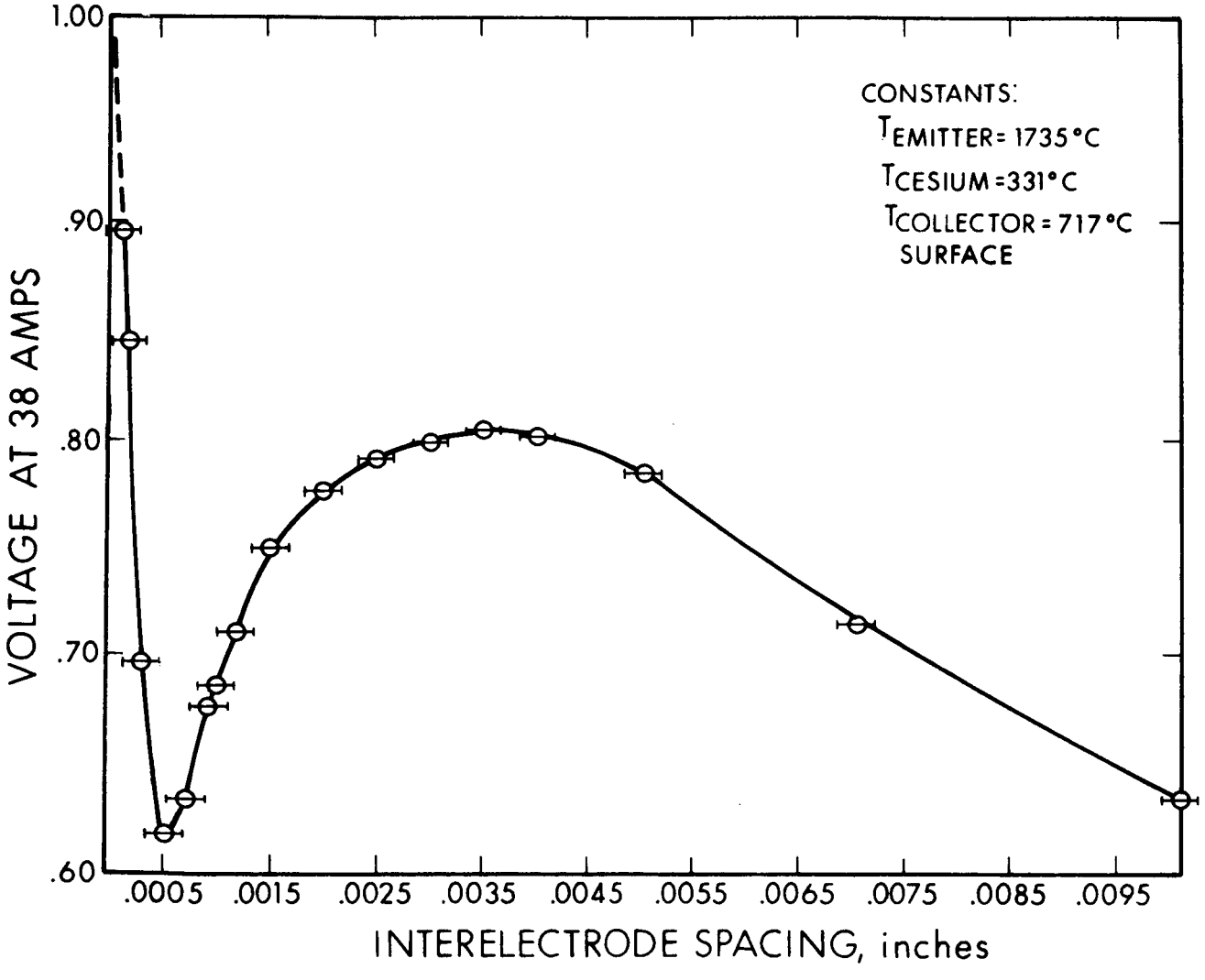

FIG. 3-2 INTERELECTRODE SPACING VERSUS VOLTAGE; EMITTER, COLLECTOR, AND CESIUM RESERVOIR TEMPERATURES CONSTANT (all dc data points)

invariable at approximately 16 mil-torr within the limits of experimental error. Figures 3-3 through 3-9 show the data acquired in the low emitter temperature region. All data plotted are dc data taken under steady-state conditions of operation. It is interesting to note the continuous depression of the voltage minimum in these data as a function of decreasing emitter temperature, an example of losing contact potential difference between emitter and collector. In fact, it may be seen that at the condition of very low emitter temperatures and close spacing a voltage must be applied to support the electron current flow between emitter and collector.

Table 3-1 summarizes the pd products from these curves with three additional sets of data included from previous investigations (Ref. 3). The average pd product from these data is computed to be 16.0 mil-torr ±0.8 mil-torr. It may be noted from the curves and the tabulated data that the pd product is independent of emitter temperature. The optimum pd product is also independent of the collector material as shown in Fig. 3-10, the comparison curve of the Re-Re and Re-Mo systems. Although there is a difference in the maximum voltage outputs, the maxima occur at the identical spacing.

From these preliminary measurements, it appears that the pd product of 16 mil-torr ±0.8 mil-torr is a constant for thermionic converters regardless of emitter material, collector material, or range of temperature operation. It may be further inferred from these data that the ionization processes in an arc-mode converter occur in the volume between electrodes both at high and low emitter temperatures.

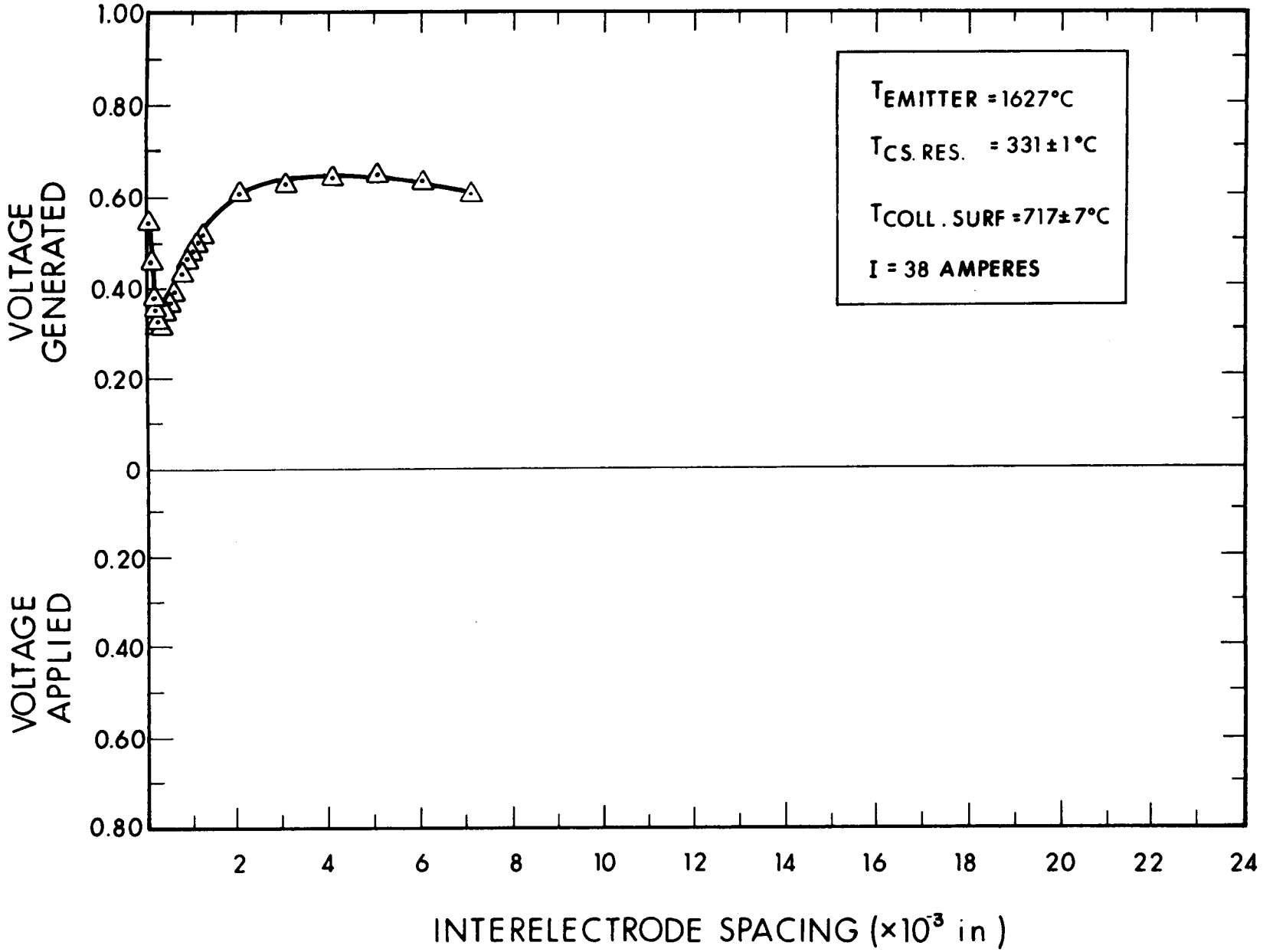

FIG. 3-3 VOLTAGE OUTPUT VERSUS INTERELECTRODE SPACING RELATIONSHIP FOR T_E = 1627°C, NONOPTIMIZED FOR PERFORMANCE OUTPUT (all points are dc data)

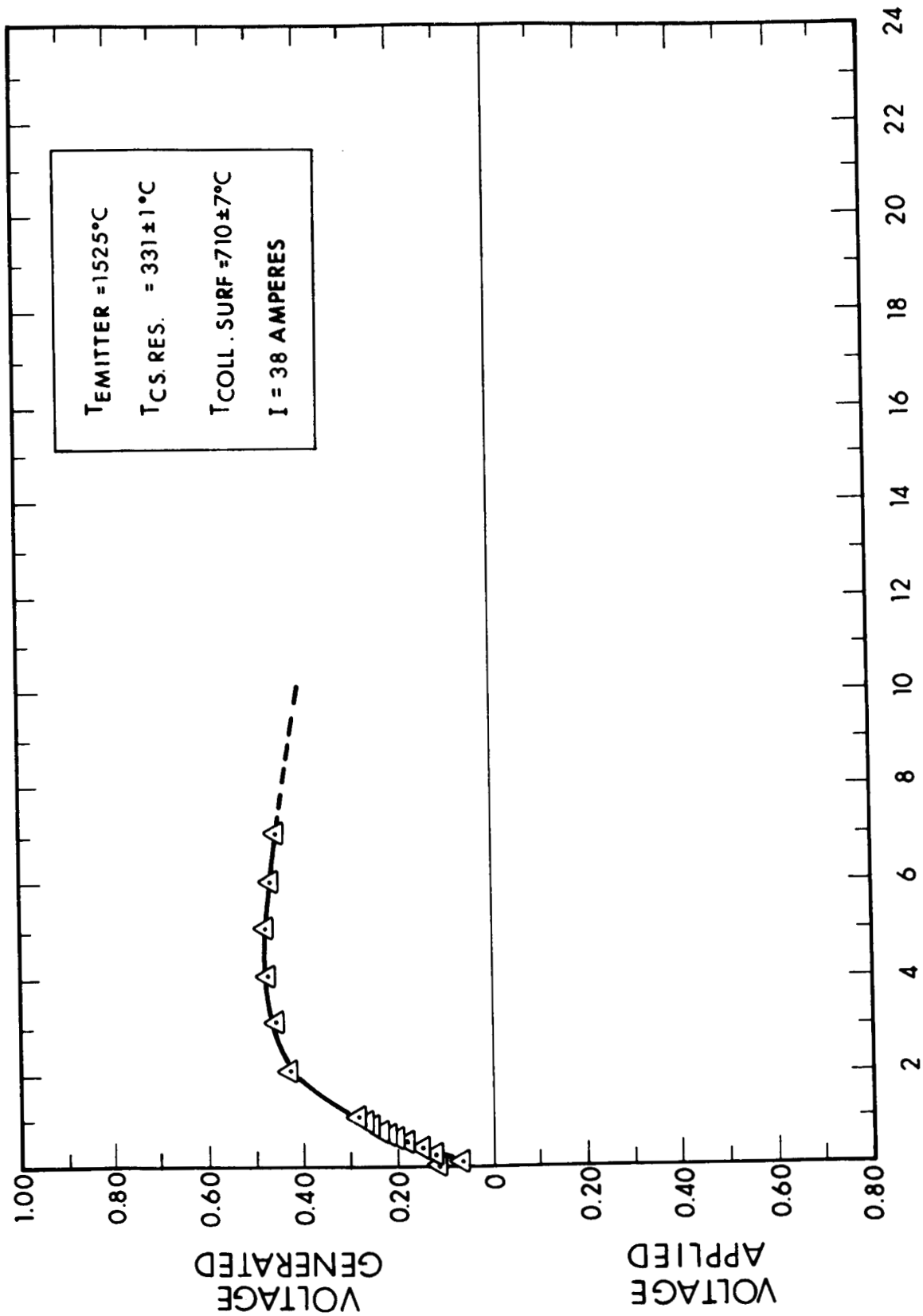

FIG. 3-4 VOLTAGE OUTPUT VERSUS INTERELECTRODE SPACING FOR T_E = 1525°C, NONOPTIMIZED PERFORMANCE (all points are dc data)

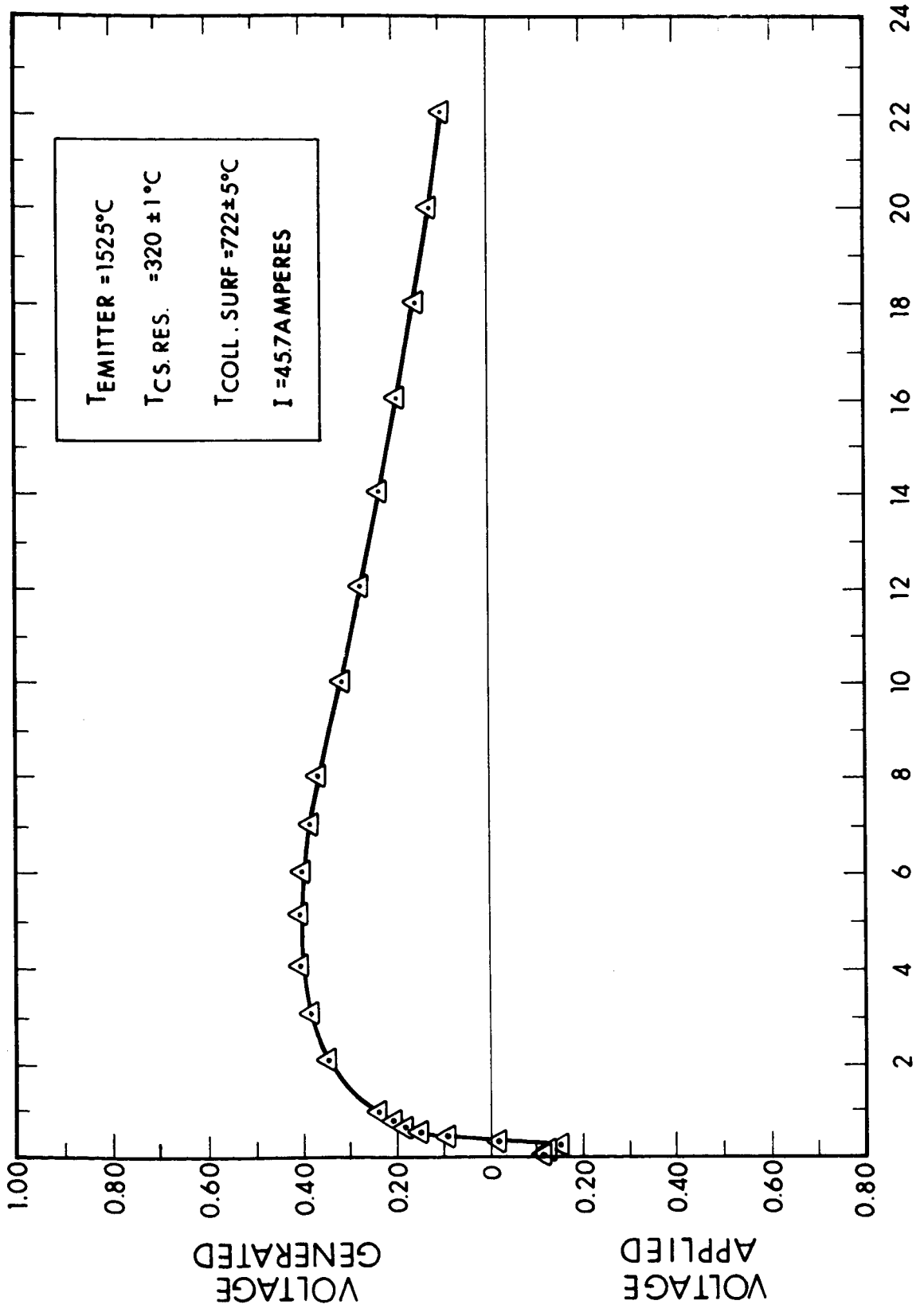

FIG. 3-5 VOLTAGE VERSUS INTERELECTRODE SPACING RELATIONSHIP FOR T_E = 1525°C, OPTIMIZED FOR 0.40 VOLT OUTPUT (all points dc data)

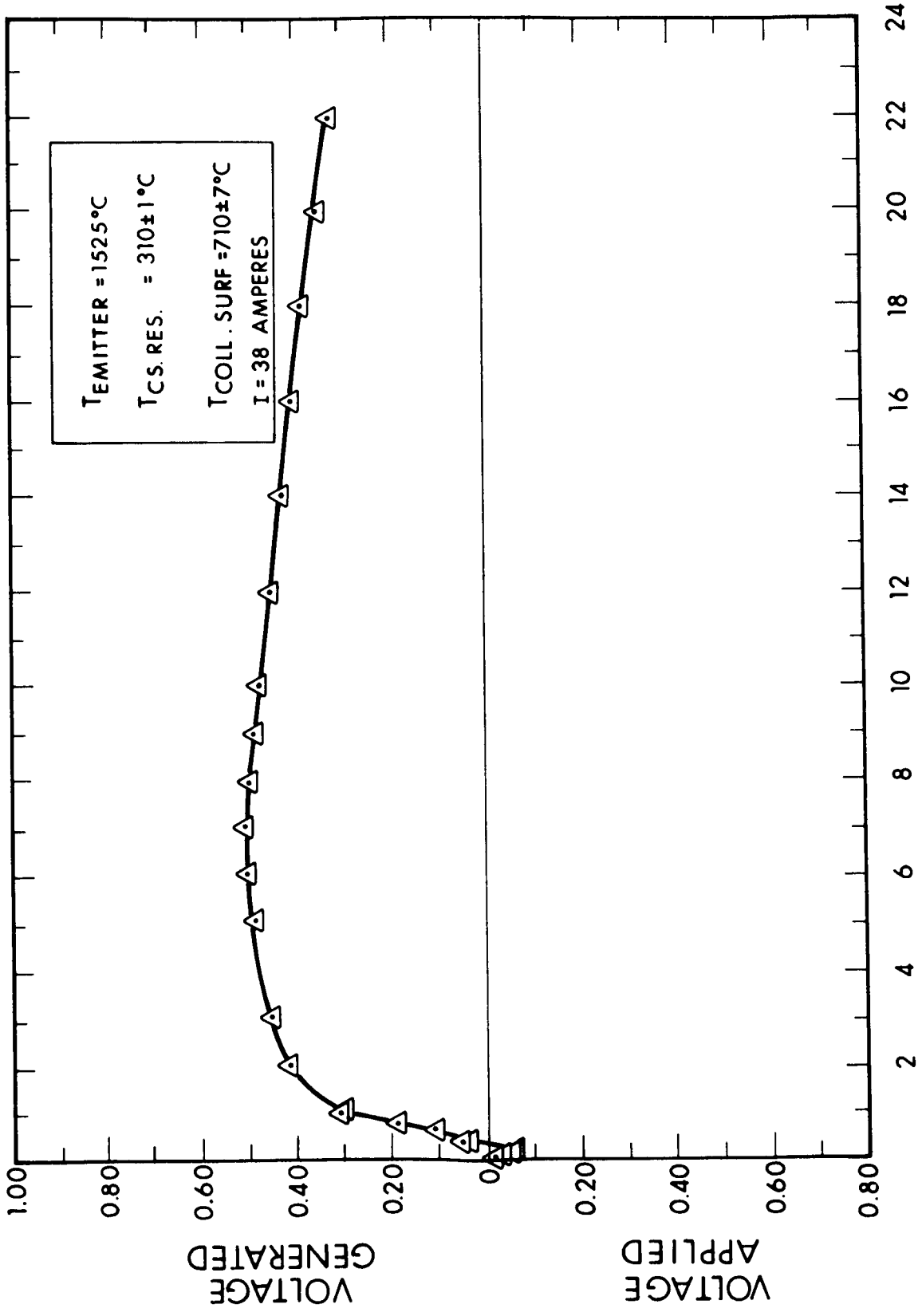

FIG. 3-6 VOLTAGE VERSUS INTERELECTRODE SPACING RELATIONSHIP FOR T_E = 1525°C, OPTIMIZED FOR 0.5 VOLT OUTPUT (all points dc data)

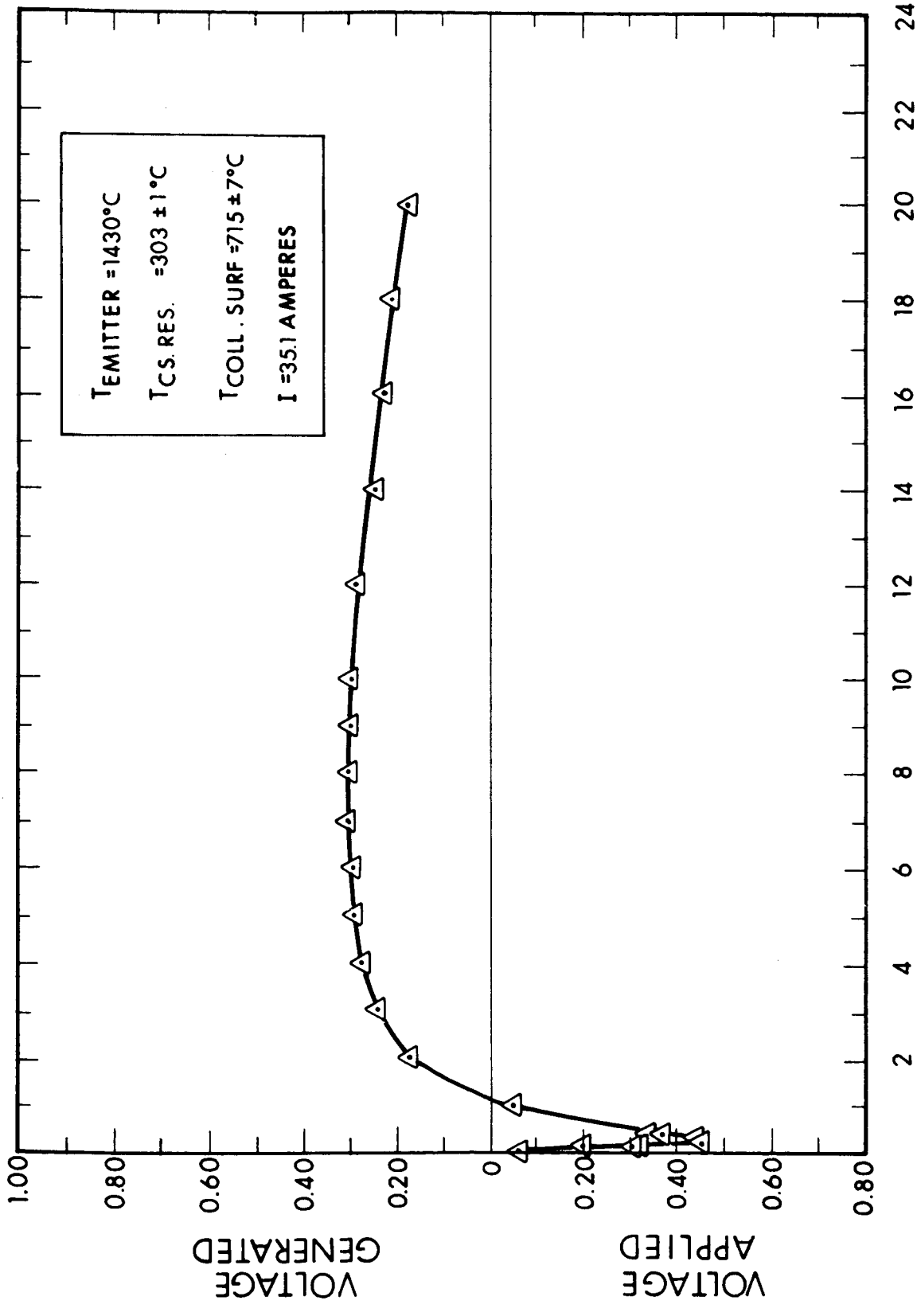

FIG. 3-7 VOLTAGE VERSUS INTERELECTRODE SPACING RELATIONSHIP FOR T_E = 1430°C, OPTIMIZED FOR 0.3 VOLT OUTPUT (all points dc data)

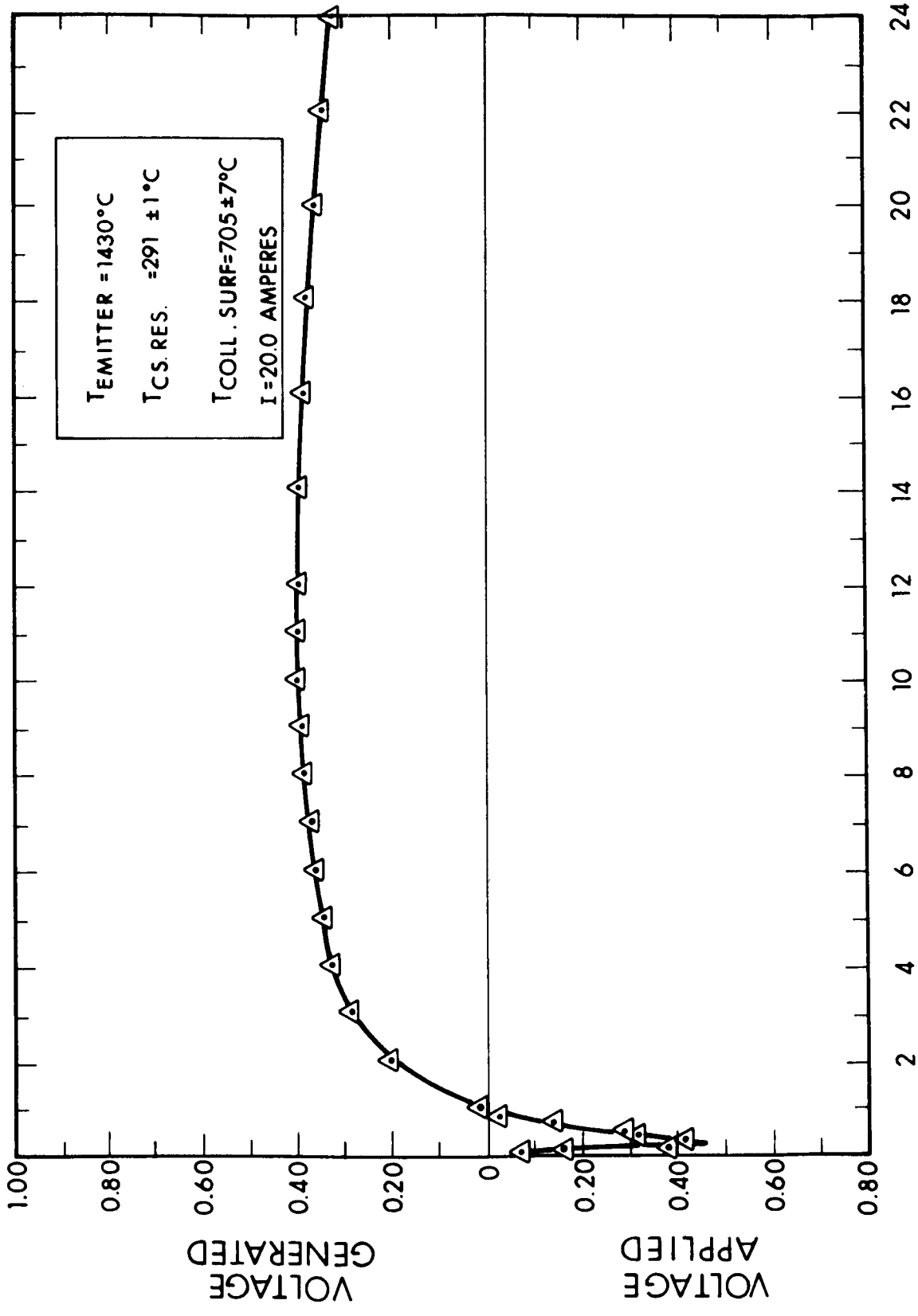

FIG. 3-8 VOLTAGE VERSUS INTERELECTRODE SPACING RELATIONSHIP FOR T_E = 1430°C, OPTIMIZED FOR 0.40 VOLT OUTPUT (all points dc data)

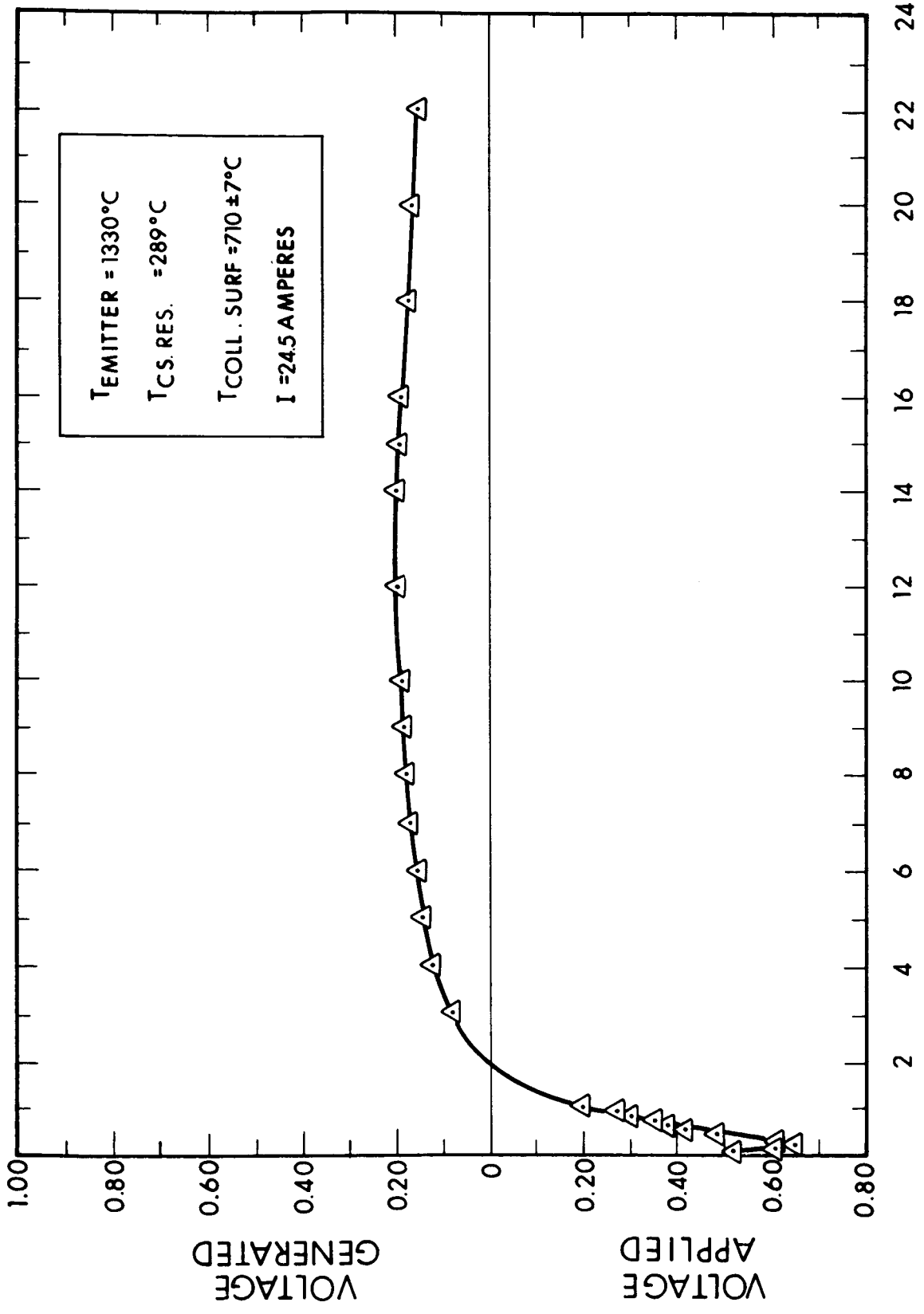

FIG. 3-9 VOLTAGE VERSUS INTERELECTRODE SPACING RELATIONSHIP FOR T_E = 1330°C, OPTIMIZED FOR 0.20 VOLT OUTPUT (all points are dc data)

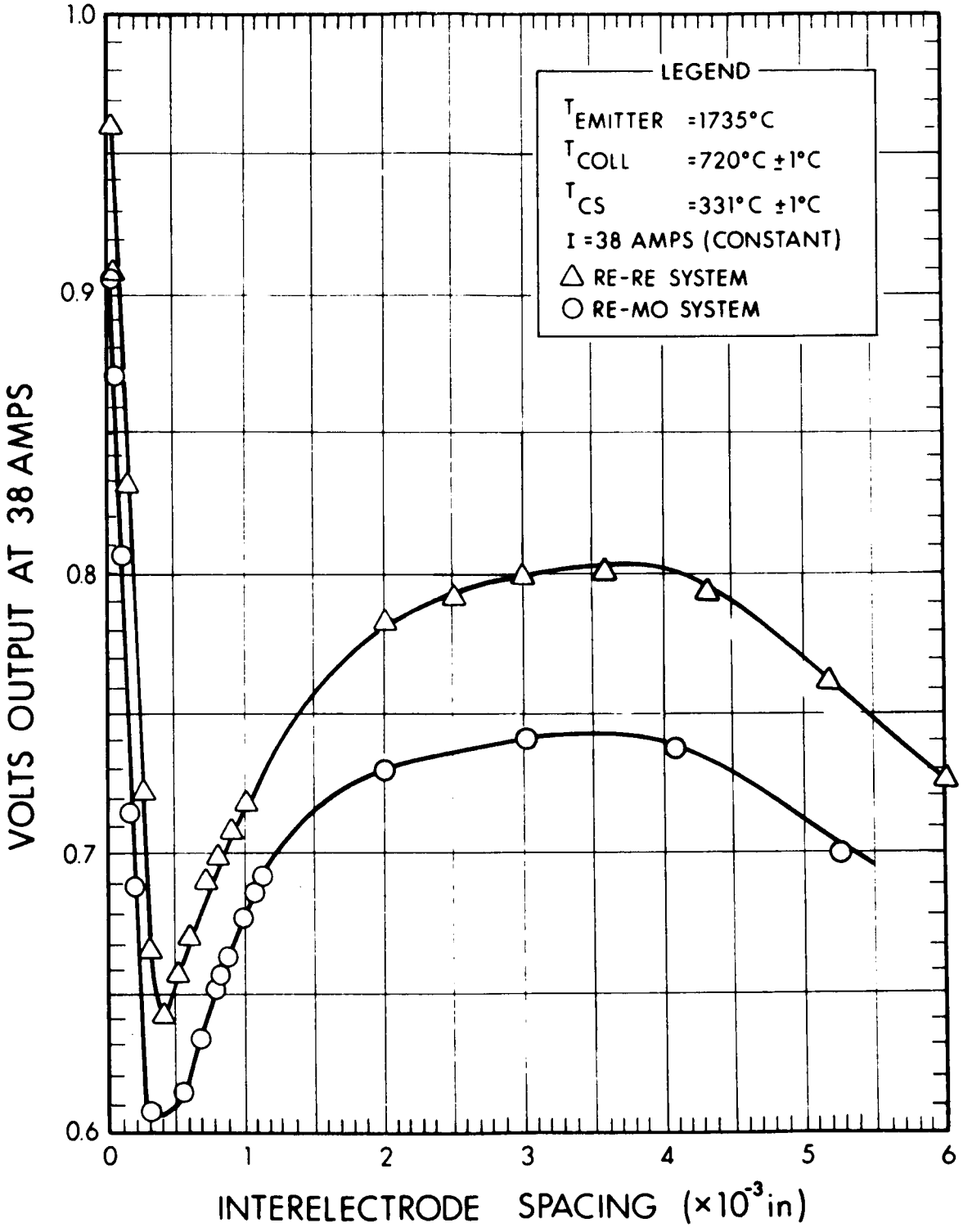

FIG. 3-10 COMPARISON PLOT OF Re-Re SYSTEM TO Re-Mo SYSTEM SHOWING VOLTAGE OUTPUT DIFFERENCE OF 60 TO 80 mW OVER ENTIRE SPACING RANGE

TABLE 3-1

SUMMARY OF PRESSURE-DISTANCE DATA

$T_{emitter}$	$T_{cs\ res}$	P_{cs}	pd
1327°C	289°C	1.33 torr	16.7 mil-torr
1427°C	291°C	1.43 torr	15.7 mil-torr
1427°C	303°C	1.96 torr	15.6 mil-torr
1527°C	310°C	2.35 torr	16.8 mil-torr
1527°C	320°C	3.01 torr	15.9 mil-torr
1527°C	331°C	4.02 torr	15.7 mil-torr
1627°C	331°C	4.02 torr	15.7 mil-torr
1735°C	331°C	4.02 torr	15.7 mil-torr
1735°C	344°C	5.30 torr	15.9 mil-torr
1735°C	350°C	6.06 torr	16.3 mil-torr

3.2 SIGNIFICANCE OF A MINIMUM COLLECTOR WORK FUNCTION

Figure 3-10 is representative of the central thesis of this program: namely, the demonstration of increased thermionic converter performance attributable to a minimum collector work function. An average difference of 70-80 millivolts between the two sets of data is readily seen at the optimum spacing of 3.8 to 3.9 mils. At closer spacings of 1-2 mils the voltage difference is somewhat less, possibly because the collector temperature is difficult to control in this region which can account for 0.1-0.2 mil changes in the spacing. At the very close spacings of less than 0.0005 inch the collector temperature is easily controlled and the voltage difference is again near 70-80 millivolts. Since the electron current flow and electrode surface temperatures are maintained constant while taking data from the vehicle, the only varying heat transfer quantity to the collector is gas atom conduction. The problem of controlling the collector

temperature as a function of interelectrode spacing is: at very close spacings the heat transfer by cesium atom gas conduction is spacing independent and follows the classical laws developed by Knudsen, at spacings from 0.5 to 2.0 mils, heat transfer measurements suggest that cesium atom gas conduction is spacing dependent, and finally, at larger spacings the heat transfer by gas atom conduction is constant.

Collector work function measurements were taken from the test vehicle in both the molybdenum and the rhenium-on-molybdenum configurations, the difference between the two being 70 to 80 millivolts. Therefore, from two independent sets of measurements (viz., voltage output versus interelectrode spacing and saturated emission) the lower value of collector work function leads to higher power output.

In addition to the data from the test vehicles, two planar thermionic converters were fabricated and tested during a previous program which verified the observation of increased power output resultant from a lower collector work function. Both converters were built to operate at a fixed interelectrode spacing of 3.8 mils, one of which had a rhenium emitter and rhenium collector, the other a rhenium emitter and molybdenum collector. At 0.8 Vdc the rhenium-rhenium configuration output is 15.2 to 15.3 watts/cm^2 versus 13.6 to 13.7 watts/cm^2 for the rhenium-molybdenum configuration, a 10 percent increase. At 0.7 Vdc the performance is 21.0 watts/cm^2 in the rhenium-rhenium system as opposed to 18.6 watts/cm^2 from the rhenium-molybdenum system, a 12 percent increase. The increase in converter power output, Δp, due to a decrease in collector work function, ΔE, at constant current is given by

$$\Delta p = I\Delta E, \text{ since } \Delta I = 0$$

or

$$\frac{\Delta p}{p} = \frac{\Delta E}{E}$$

since $p = IE$.

For ΔE = 80 millivolts (the difference between a rhenium collector surface and a molybdenum collector surface), the increase in power output at 0.8 Vdc is $\frac{0.080}{0.80}$ = 10 percent, the increase at 0.7 Vdc is $\frac{0.080}{0.70}$ = 12 percent, both of which agree with the aforementioned measurements. As a point of interest to low temperature thermionics, where the converter voltage output may be in the 0.4V to 0.5V range, it is readily seen that the advantage of a rhenium collector surface over a molybdenum collector surface is 15 percent more output at 0.5 volt and 20 percent more output at 0.4 volt.

In terms of the present program, an oriented vapor-deposited coating of rhenium free from processing contaminants such as fluorides or chlorides would yield a minimum cesiated work function of about 1.35 volts. In turn, this is approximately an increase of 80 to 90 millivolts of voltage output over an ordinary polycrystalline rhenium collector surface. For a low temperature converter operating at 0.5V output, an oriented vapor-deposited rhenium collector substrate could produce 40 percent higher output power than a polycrystalline molybdenum collector substrate. The estimate of 1.35 volts is based on two assumptions which are: (1) a bare work function or vacuum work function of 5.1-5.3 volts for oriented vapor-deposited rhenium, and (2) existence of the same trend between bare work function and minimum cesiated work function which has been experimentally observed for Nb, Mo, and Re.

As a final part of the effort directed toward evaluating electrode materials, a comparison of the optimized performance available from a cesiated rhenium collector converter system was made with the optimized performance from an oxygen additive system. The data for the oxygen additive system was obtained from the final report on JPL Contract 951262 and is shown in Fig. 3-11 along with cesium-only data taken from the EOS variable parameter test vehicle. The emitter

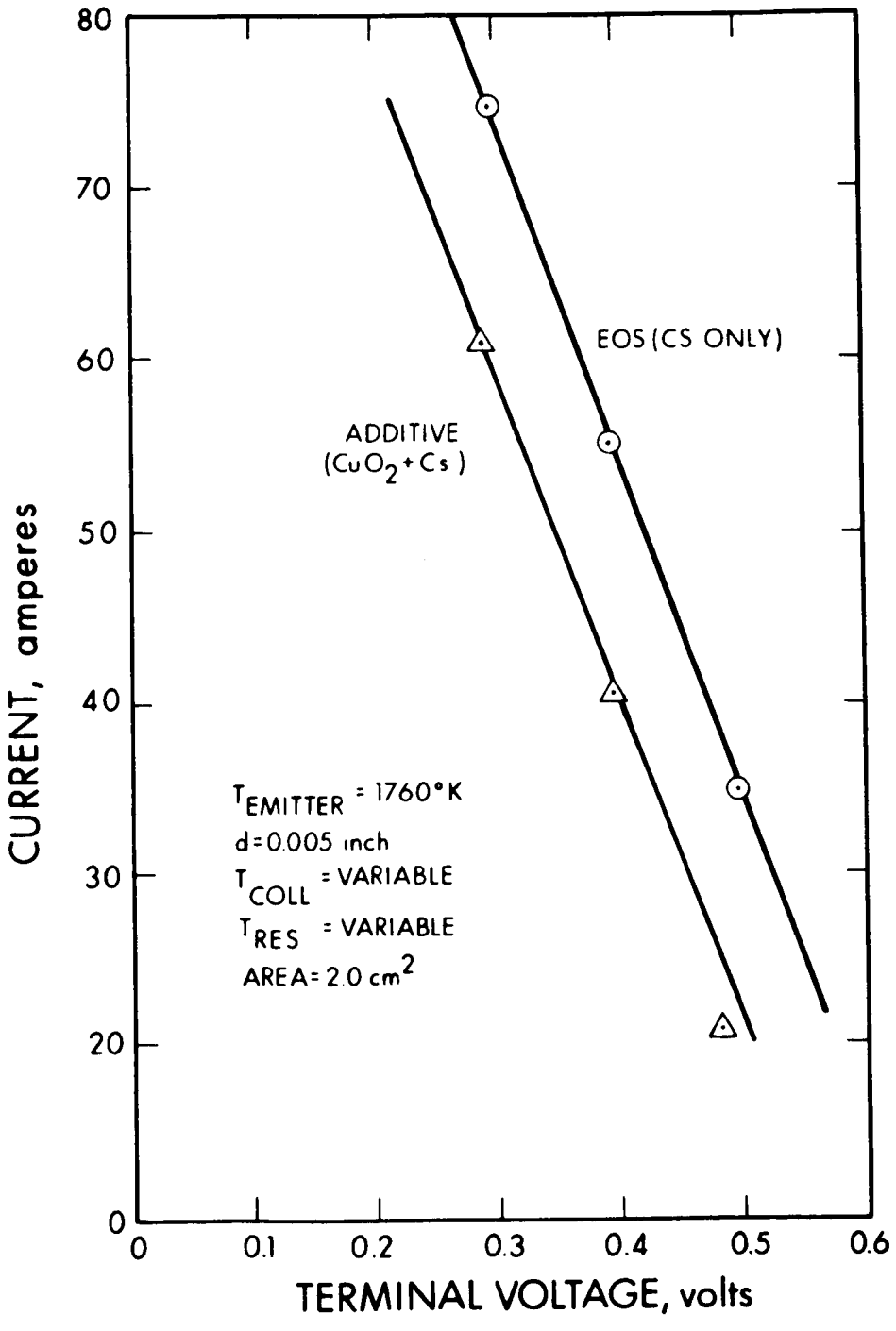

FIG. 3-11 OPTIMIZED PERFORMANCE PLOT COMPARING ADDITIVE DATA TO EOS NONADDITIVE DATA

temperature, in both cases, is the emitter surface temperature; the voltage output, in both cases, is the terminal voltage; and finally, the spacing, in both cases, is 5 mils. In each case, the collector and cesium reservoir temperatures are optimized for maximum output. The additive system employs tungsten-molybdenum electrodes while the cesium-only system employs rhenium-rhenium electrodes, and herein lies the important difference between the two. The rhenium collector provides the lower collector work function and consequently better performance. In fact, 80 millivolts more voltage output was observed on the rhenium collector system at each current level from 20 to 70 amperes than was reported on the additive system.

During the course of the VPTV evaluation of vapor-deposited rhenium further comparisons will be made between the additive and nonadditive systems. At the present, however, as Fig. 3-11 indicates, greater performance is available from the simpler polycrystalline rhenium collector system than from any other known thermionic converter collector except perhaps an oriented or single crystal collector. The equations for increased output which were discussed previously are still applicable here; for example, the expected increase in output at 0.4 volt is $\frac{0.080}{0.40}$ = 20 percent. From the figure, the additive data yield 41 amps at 0.4V or 8.2 watts/cm^2. The EOS cesium-only converter yields 41 amps at 0.48V or 9.8 watts/cm^2, a 20 percent increase over 8.2 watts/cm^2. If, instead of holding the current level constant, the voltage level is held constant, then the increase of the nonadditive system over the additive system is 35 percent.

3.3 OPTIMIZED CONVERTER PERFORMANCE AT LOW EMITTER TEMPERATURES FOR THE RHENIUM-RHENIUM ELECTRODE SYSTEM

Summarized in this section is the optimized converter performance at low emitter temperatures ($\leq 2000^{\circ}K$) from the variable parameter test vehicle in the rhenium-rhenium electrode configuration. The data, shown in Figs. 3-12 through 3-16, should be reviewed with the following in mind:

a. All output current and voltage is dc steady-state as observed on 0.1 percent accurate meters. Voltage output is measured at the converter terminals.

b. All emitter temperatures are measured with a calibrated micro-optical pyrometer sighted on a 10:1 depth-to-diameter hohlraum. The temperatures quoted are true hohlraum, not surface corrected.

c. The active emitter area is 2.0 square centimeter as determined by a guarded collector.

d. Interelectrode spacings were determined with ±0.1 mil dial indicators.

e. The dc output was reproducible within 1 to 2 percent over the 1000 hours of test vehicle operation before delivery to JPL.

The power output at $1527^{\circ}C$ (true hohlraum) is 7.2 watts/cm^2 at 0.5V; 9.2 watts/cm^2 at 0.4V; and 10.5 watts/cm^2 at 0.35V. The power output at $1427^{\circ}C$ (true hohlraum) is 4.1 watts/cm^2 at 0.4V and 5.4 watts/cm^2 at 0.3V.

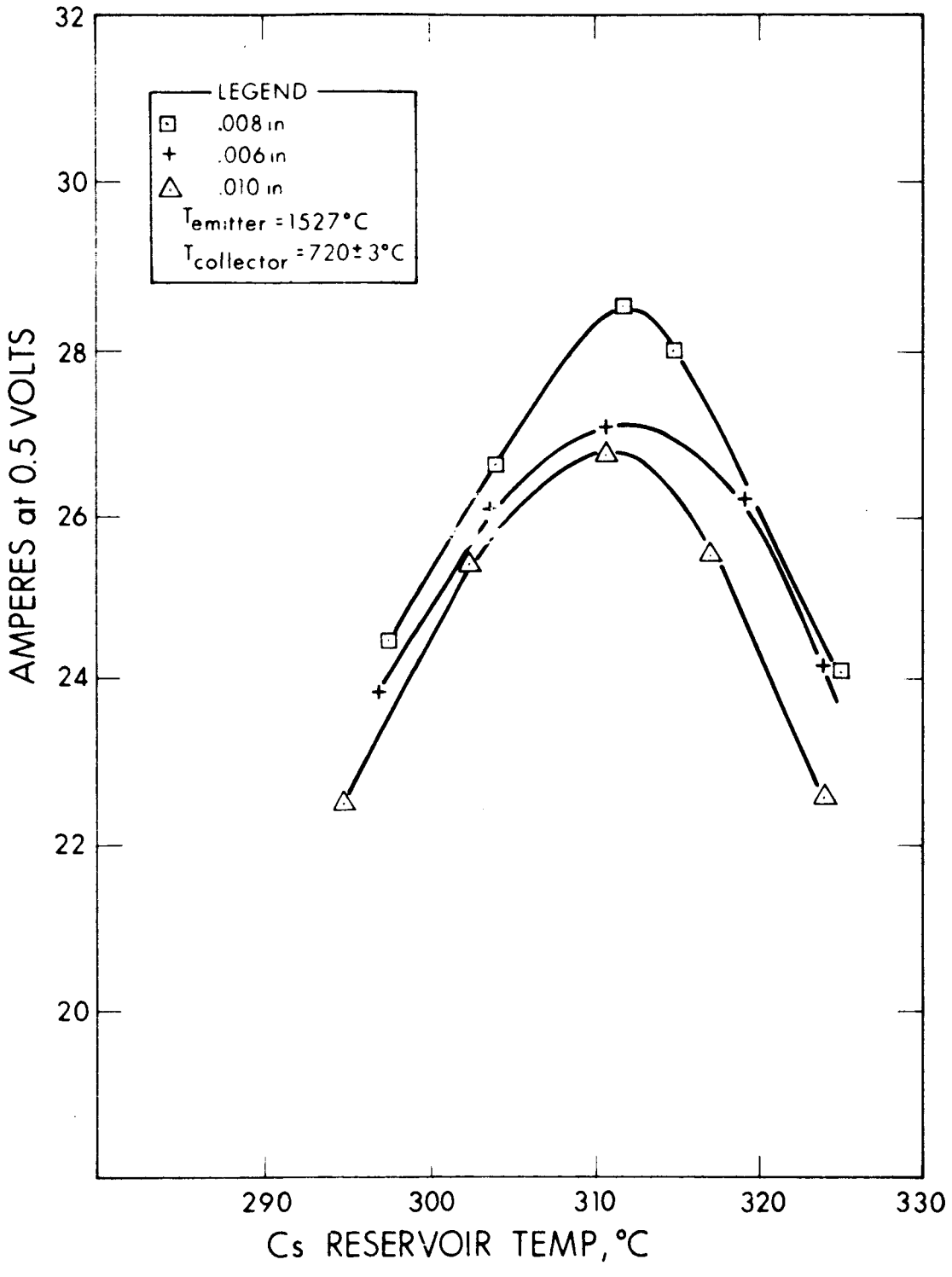

FIG. 3-12 CURRENT AT 0.5 VOLT VERSUS CESIUM RESERVOIR TEMPERATURE FOR T_E = 1527°C

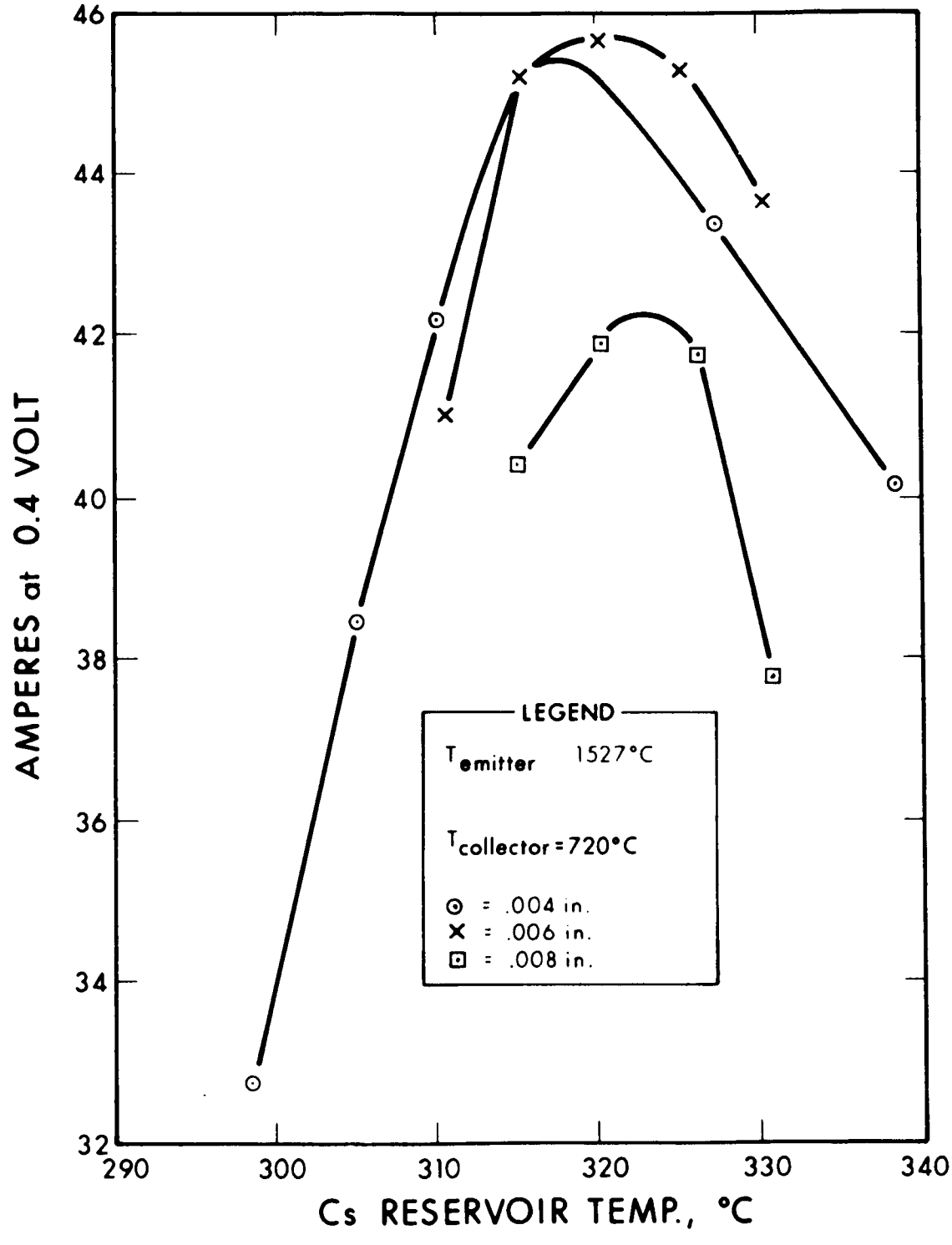

FIG. 3-13 CURRENT AT 0.4 VOLT VERSUS CESIUM RESERVOIR TEMPERATURE AT T_E = 1527°C

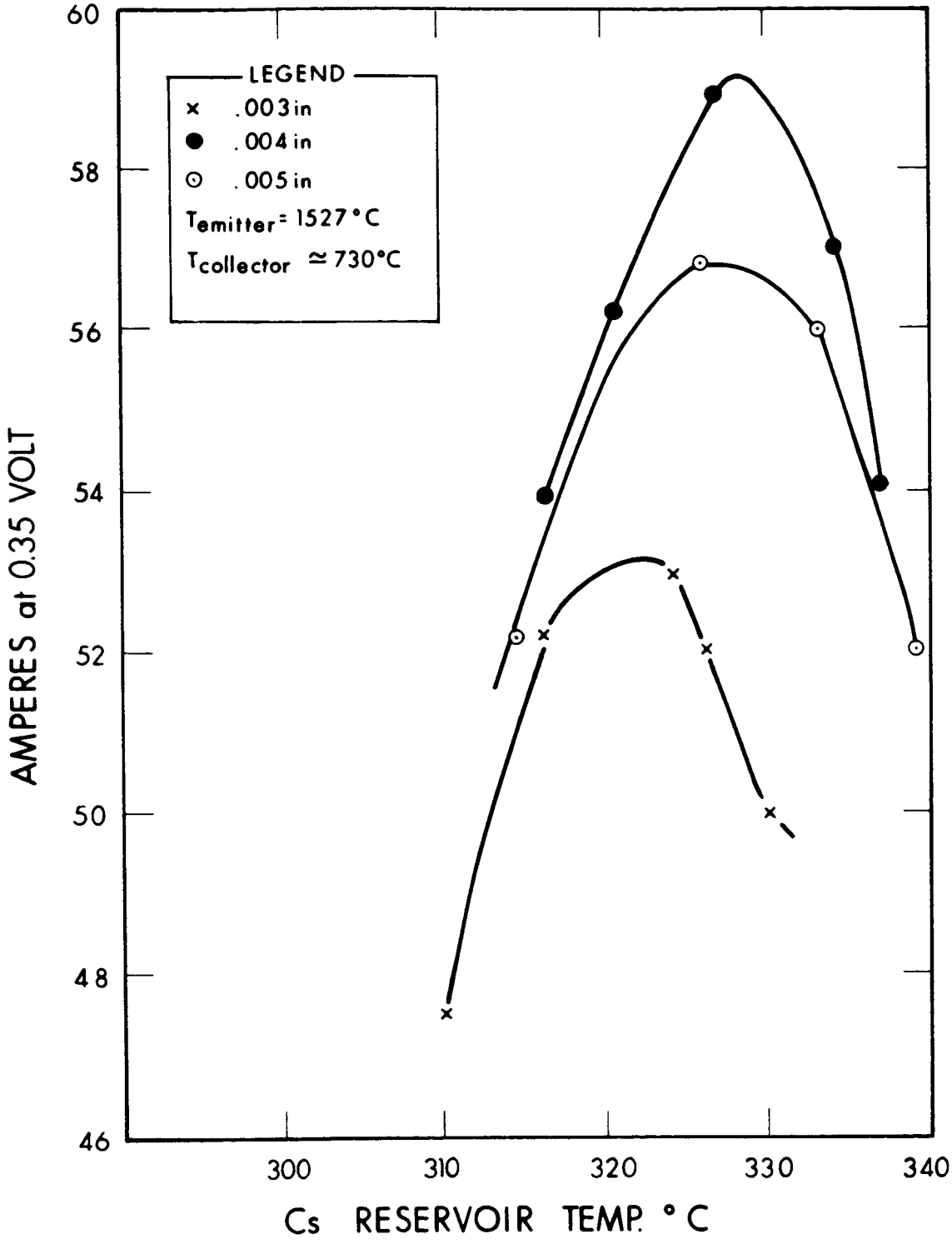

FIG. 3-14 CURRENT AT 0.35 VOLT VERSUS CESIUM RESERVOIR TEMPERATURE AT T_E = 1527°C

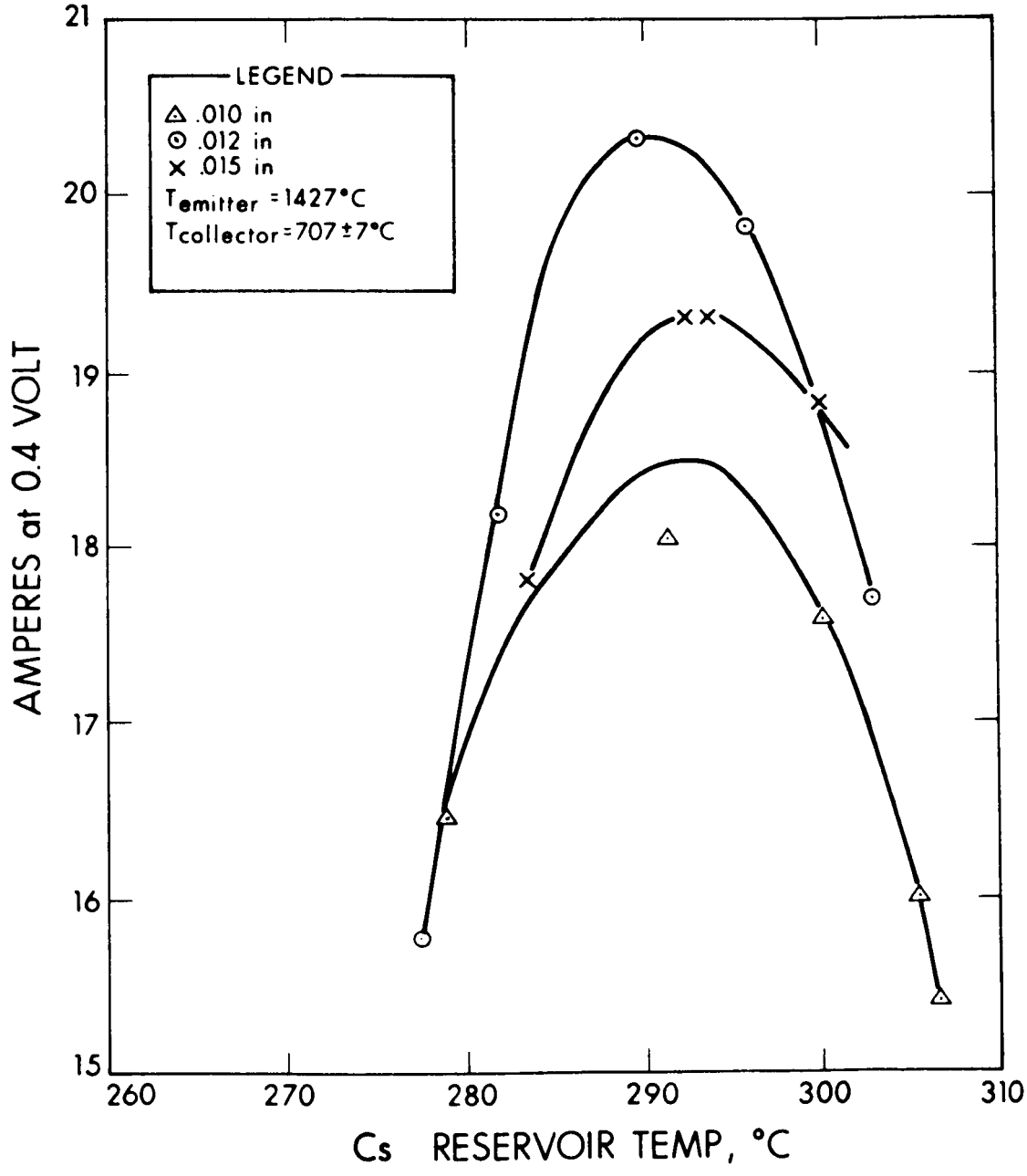

FIG. 3-15 CURRENT AT 0.4 VOLT VERSUS CESIUM RESERVOIR TEMPERATURE AT T_E = 1427°C

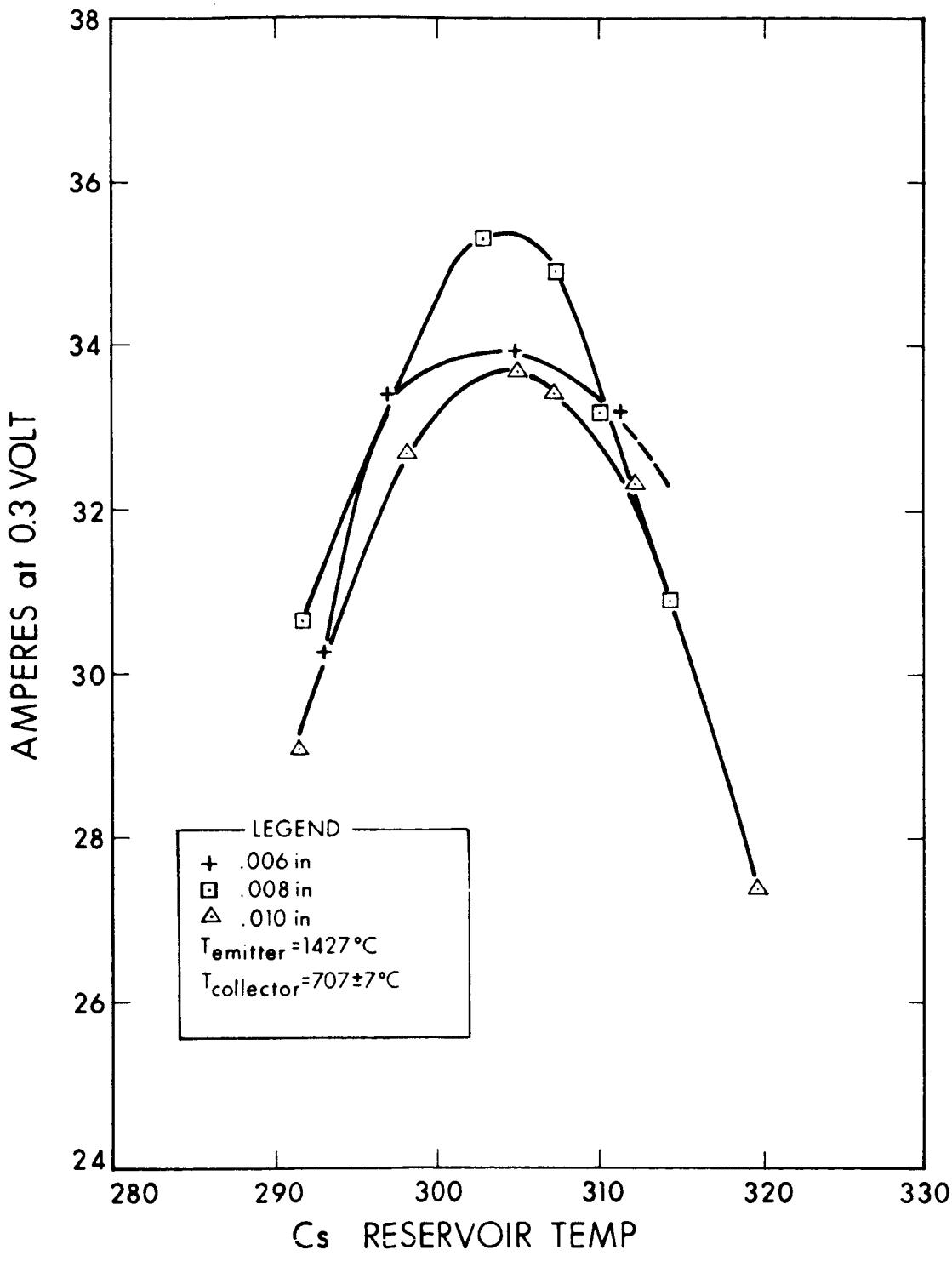

FIG. 3-16 CURRENT AT 0.3 VOLT VERSUS CESIUM RESERVOIR TEMPERATURE AT T_E = 1427°C

SECTION 4

ANALYSIS AND INTERPRETATION (TASK III)

4.1 INTRODUCTION

The primary objective of Task III is to formulate a theoretical description of thermionic converter performance and apply it to an analysis and correlation of the parametric vehicle data of Task II and the data acquired in Task I. Specific topics that will receive particular attention in this task are: (1) the similarity laws of a cesium vapor discharge, (2) the ionization mechanisms in a cesium plasma, and (3) the characteristics of the collector sheath. Task III will proceed in roughly three stages, each stage covering one of the regions of parametric vehicle operation as defined by the typical output voltage interelectrode spacing curve, V(d), shown in Fig. 4-1.

Region I of Fig. 4-1 is designated the electron space charge region and extends from zero interelectrode spacing to the minimum of V(d) identified as the plasma onset point. In region I, the output voltage at small interelectrode spacings is governed primarily by space charge created by electrons emitted by both emitter and collector in the absence of significant numbers of cesium ions. The theoretical model adapted for the first analysis of this region is the double vacuum diode. This model is undoubtedly valid at very small spacings, but it will have to be augmented as the spacing approaches the onset point from below by including the influences of excited cesium atoms and cesium positive ions.

At interelectrode spacings near the plasma onset point and above, the voltage output curve begins to display characteristics of a cesium

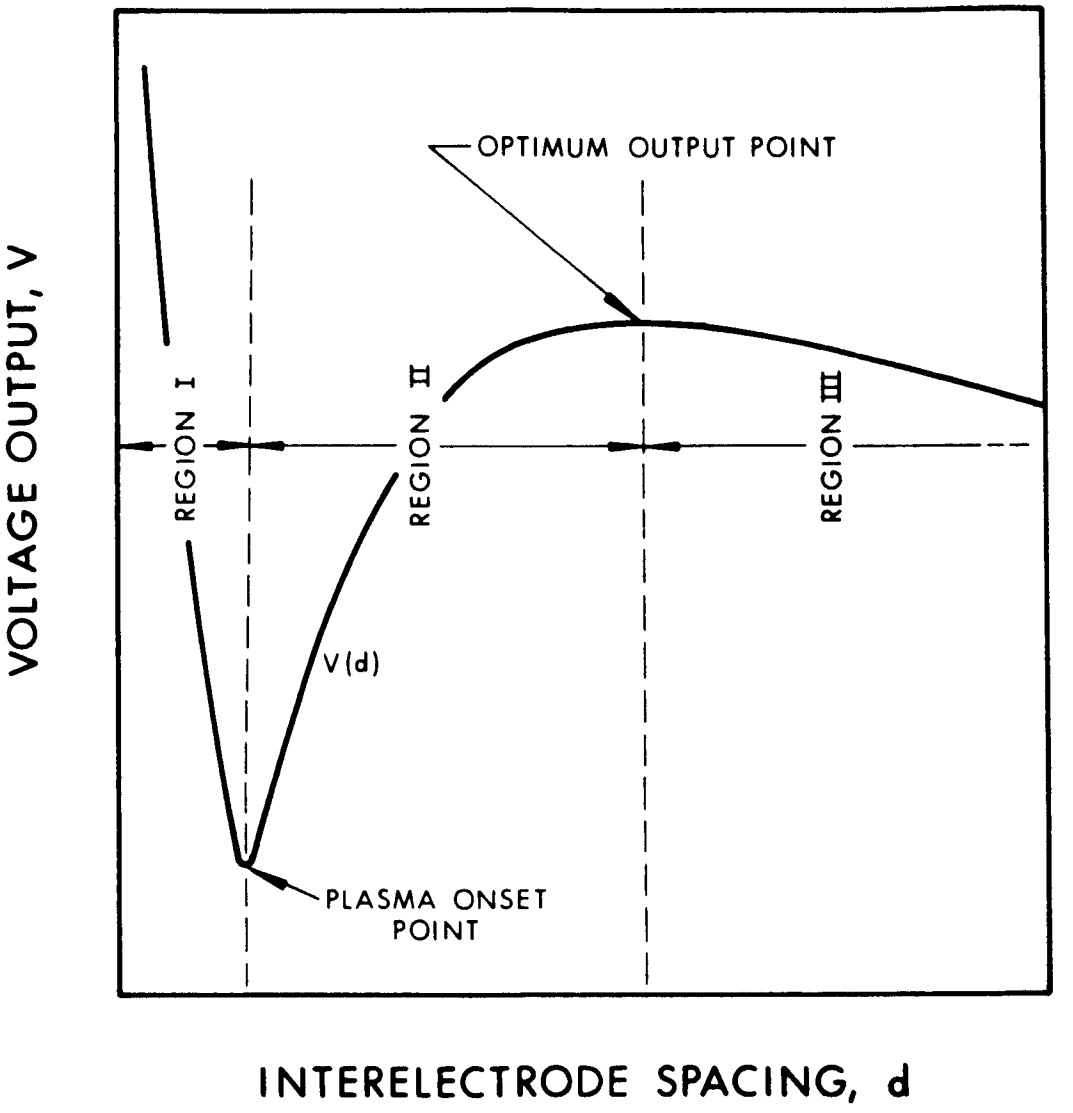

FIG. 4-1 TYPICAL VOLTAGE OUTPUT VERSUS INTERELECTRODE SPACING CURVE SHOWING THE THREE CHARACTERISTIC REGIONS DESCRIBED IN THE TEXT

plasma diode. For this reason, region II between the plasma onset point and the maximum of V(d) (identified as the optimum output point in Fig. 4-1) is designated the transition region. It is in this region that the plasma becomes fully developed. Region III is defined by the remaining portion of the output curve beyond the optimum power point and is designated the positive column region.

During this report period, the Task III effort was directed mainly to the analysis of region I. The literature on both single and double vacuum planar diode space charge has been reviewed, and specific application of double diode space charge theory to close-spaced cesium diodes is complete. The approach is similar to that of Dugan (Ref. 4).

4.2 THEORY OF THE VACUUM DOUBLE DIODE

The analytical problem consists of (1) deriving an expression for the electron space charge density in the interelectrode space due to electron emission from the electrodes, both of which are partially coated with cesium, and (2) combining this expression with Poisson's equation to derive the electrostatic potential energy as a function of position in the interelectrode space. The problem is treated in one dimension, the emitted electrons are assumed to be Maxwellian and the flow, collisionless. For a double vacuum diode operating in a region of applied positive voltage, the electrostatic potential will have the form shown schematically in Fig. 4-2. Although the space charge potential shown in Fig. 4-2 is typical of a diode operating with an applied voltage, the analysis of Task III will include the more conventional diode operation in the power producing quadrant. In that case, the Fermi level of the collector will be below the Fermi level of the emitter in Fig. 4-2.

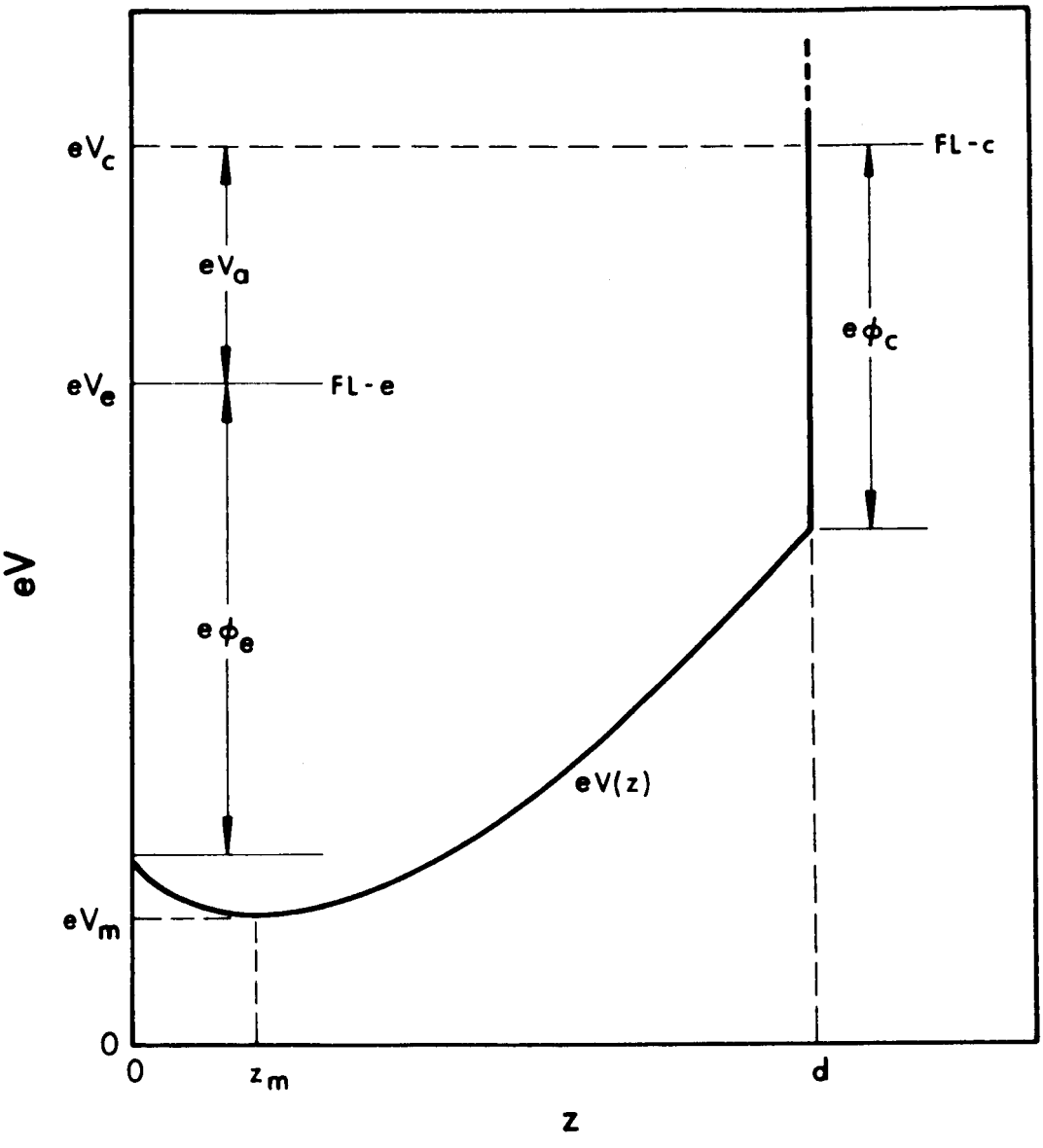

FIG. 4-2 SCHEMATIC REPRESENTATION OF THE ELECTROSTATIC POTENTIAL ENERGY DUE TO ELECTRON SPACE CHARGE BETWEEN EMITTER AND COLLECTOR

The symbols used in Fig. 4-2 and in the following discussion are listed in Table 4-1.

4.2.1 ELECTRON SPACE CHARGE IN A DOUBLE DIODE

At the emitter (z = 0: refer to Fig. 4-2), the complete Maxwellian velocity distribution of the electrons is:

$$F(u,v,w) = n_{eo}(m/2\pi kT_e)^{3/2} \exp\left[-m(u^2 + v^2 + w^2)/2kT_e\right], \qquad (1)$$

where u,v, and w are the x,y, and z components, respectively, of the electron velocity, F(u,v,w) is the number of electrons in the incremental velocity range dudvdw, and n_{eo} is the equilibrium electron density. The density, n_{eo}, is related to the work function of the emitter and the absolute temperature by

$$n_{eo} = (2/h^3)(2\pi mkT_e)^{3/2} \exp(-e\varphi_e/kT_e). \qquad (2)$$

This density is used appropriately when no electron current is being drawn from the emitter, a case approached in principle only when $V_e - \varphi_e - V_m \to \infty$. When the potential distribution in the interelectrode space is such that all electrons emitted are drawn away from the emitter without return ($V_m = V_e - \varphi_e$) the electron density will be (1/2) n_{eo}. In this case the velocity distribution will contain all values of u and v from $-\infty$ to $+\infty$ but will contain w components from 0 to $+\infty$ only. For intermediate cases such as the one depicted in Fig. 4-2 where some emitted electrons are returned to the emitter because of a finite potential minimum, the density at the emitter, $n_e(0)$, is

$$n_e(0) = (n_{eo}/2)\left[1 + \text{erf}\,(\eta^{1/2})\right] \qquad (3)$$

TABLE 4-1

LIST OF SYMBOLS

c	=	subscript referring to collector electrode
d	=	interelectrode spacing
e	=	subscript referring to emitter electrode: $-e$ = electron charge
h	=	Planck constant
k	=	Boltzmann constant
m	=	electron mass
$n_c(z)$	=	electron density due to electron flow from collector
$n_e(z)$	=	electron density due to electron flow from emitter
n_{cm}	=	electron density at potential minimum due to electron flow from collector
n_{em}	=	electron density at potential minimum due to electron flow from emitter
n_m	=	total electron density at potential minimum
n_{cd}	=	equilibrium electron density at collector surface
n_{eo}	=	equilibrium electron density at emitter surface
s	=	dummy variable in definition of error integral
u, v, w	=	x,y, and z components of velocity
x, y, z	=	rectangular coordinates
z_m	=	coordinate of potential minimum
$F(u,v,w)$	=	velocity distribution function
$F(u,v,w,V)$	=	total energy distribution function
J_c	=	electron current density flowing from collector
J_e	=	electron current density flowing from emitter
J	=	total electron current density
T_c	=	collector temperature
T_e	=	emitter temperature

TABLE 4-1

LIST OF SYMBOLS (contd)

$V(z)$	=	electrostatic potential
V_a	=	output or applied potential
V_c	=	electrostatic potential at the collector surface
V_e	=	electrostatic potential at the emitter surface
V_m	=	electrostatic potential at the potential minimum
α	=	ratio of emitter to collector temperature
β	=	ratio of electron densities at the potential minimum = n_{cm}/n_{em}
ϵ_o	=	permittivity of free space
η	=	dimensionless potential energy
η_c	=	dimensionless potential energy referred to collector temperature
η_e	=	dimensionless potential energy referred to emitter temperature
λ	=	Debye length for electron space charge
ξ	=	dimensionless coordinate
ξ_c	=	dimensionless coordinate of collector surface
ξ_d	=	dimensionless interelectrode spacing
ξ_e	=	dimensionless coordinate of emitter surface
φ_c	=	electron work function of collector
φ_e	=	electron work function of emitter

where

$$\eta = \left[(e/kT_e)(V_e - \varphi_e - V_m) \right] \tag{4}$$

and

$$\mathrm{erf}(\eta^{1/2}) = (2/\pi^{1/2}) \int_0^{\eta^{1/2}} \exp(-s^2)\, ds \tag{5}$$

is the error integral. Since erf (0) = 0, and erf ($+\infty$) = 1, the cases of no electron flow (equilibrium) and electron flow with no return to the emitter discussed above are satisfied by Eq. 3.

Equation 3 is the expression for the density at z = 0 only. To find the density in the interelectrode space where the potential is V(z), the distribution function is written to include the variation in potential:

$$F(u,v,w,V) = F(u,v,w) \exp \left[-(e/kT_e)(V_e - \varphi_e - V) \right], \tag{6}$$

with $V \equiv V(z)$. The electron density as a function of V(z) in the space between the emitter (z = 0) and the potential minimum ($z = z_m$) is obtained by integrating F(u,v,w,V) over all u and v from $-\infty$ to $+\infty$, and over the velocity w from $-w_1$ to ∞, where

$$\frac{mw_1^2}{2} = e(V - V_m). \tag{7}$$

The velocity w_1 is the minimum velocity in the +z direction an electron starting at the plane at z ($0 < z < z_m$) must have to pass over the potential minimum. All electrons starting in the plane at z with velocities in the +z direction greater than w_1 pass the potential minimum and proceed into the interelectrode space between z_m and the collector.

These electrons do not return to the emitter and consequently contribute to the space charge only in the region of the emitter during their transport from the emitter to z_m. Since they do not return to the emitter, the distribution of the w component of velocities at the emitter does not contain velocities greater than $|w_1|$ directed in the -z direction.

Similarly, the density of electrons in the interelectrode space between z_m and the collector (z = d) will be found by integrating Eq. 6 over all u and v, and over w from $+w_1$ to ∞. The results are:

$$n_e(z) = (n_{eo}/2) \exp\left[-(e/kT_e)(V_e-\varphi_e-V)\right]\left\{1+\mathrm{erf}\left[(e/kT_e)^{1/2}\ (V-V_m)^{1/2}\right]\right\} \quad (8a)$$

for $0 < z < z_m$, and

$$n_e(z) = (n_{eo}/2) \exp\left[-(e/kT_e)(V_e-\varphi_e-V)\right]\left\{1-\mathrm{erf}\left[(e/kT_e)^{1/2}\ (V-V_m)^{1/2}\right]\right\} \quad (8b)$$

for $z_m < z < d$. Note that Eq. 8a reduces to Eq. 3 at $V = V_e - \varphi_e$. At $z = z_m$, both Eq. 8a and Eq. 8b yield

$$n_e(z_m) \equiv n_{em} = (n_{eo}/2) \exp\left[-(e/kT_e)(V_e-\varphi_e-V_m)\right]. \quad (9)$$

It will be convenient to express Eqs. 8a and 8b in terms of n_{em} instead of n_{eo} and to use the notation

$$\eta_e = e(V-V_m)/kT_e \ . \quad (10)$$

Eqs. 8a and 8b then can be written

$$n_e(z) = n_{em}\, e^{\eta_e}\left[1 \pm \mathrm{erf}\left(\eta_e^{1/2}\right)\right], \quad (11)$$

where the positive and negative signs are for the coordinates $z \lesseqgtr z_m$ respectively.

A similar set of expressions is derived in the same manner for the electrons emitted by the collector for the space between the collector and z_m and for the space between z_m and the emitter. These are:

$$n_c(z) = n_{cm} e^{\eta_c} \left[1 \mp \text{erf}\left(\eta_c^{1/2}\right)\right] \tag{12}$$

where the negative and positive signs are for $z \lesseqgtr z_m$. The definitions of n_{cm} and η_c are analogous to n_{em} and η_e, in Eqs. 9 and 10; that is

$$\eta_c = e(V - V_m)/kT_c \tag{13}$$

and

$$n_{cm} = (n_{cd}/2) \exp\left[-(e/kT_c)(V_c - \phi_c - V_m)\right]. \tag{14}$$

The total electron density in the plane at z in the interelectrode space is the sum of the densities given by Eqs. 11 and 12. Letting

$$\beta = n_{cm}/n_{em} \tag{15}$$

and writing

$$T_c = (1/\alpha)\, T_e \tag{16}$$

so that $\eta_c = \alpha\eta_e$, the total electron density, n(z), is

$$n(z) = n_{em}\left\{e^{\eta}\left[1 \pm \text{erf}\left(\eta^{1/2}\right)\right] + \beta e^{\alpha\eta}\left[1 \mp \text{erf}\left(\alpha^{1/2}\,\eta^{1/2}\right)\right]\right\} \tag{17}$$

The subscript e has been dropped from η since η now refers only to the emitter and is defined by Eq. 10.

4.2.2 POISSON'S EQUATION FOR THE DOUBLE DIODE

Poisson's Equation,

$$d^2V/dz^2 = (e/\epsilon_o)n \tag{18}$$

where $n \equiv n(z)$, can be written in dimensionless form by using η as the dependent variable throughout and replacing the z coordinate by

$$\xi = (z-z_m)/\lambda \tag{19}$$

where λ is the Debye length for electron space charge. λ is given by

$$\lambda = (\epsilon_o kT_e/e^2 n_{em})^{1/2} \tag{20}$$

which, for n_{em} in $(\text{meters})^{-3}$ and λ in meters, is

$$\lambda = 69.0\ (T_e/n_{em})^{1/2}$$

It is frequently useful to express λ in terms of the total electron density at the space charge minimum, n_m $(=n_{em} + n_{cm})$. Equation 20 is then

$$\lambda = [\epsilon_o kT_e(1 + \beta)/e^2 n_m]^{1/2}$$

in the notation used here.

The final dimensionless form of Poisson's equation is

$$d^2\eta/d\xi^2 = e^{\eta}\left[1 + \text{erf}(\eta^{1/2})\right] + \beta e^{\alpha\eta}\left[1 \mp \text{erf}(\alpha^{1/2}\eta^{1/2})\right] \tag{21}$$

where the positive and negative signs are for $\xi \gtrless 0$.

4.2.3 COMPUTER SOLUTIONS OF POISSON'S EQUATION

Although Poisson's equation in the form of Eq. 21 can be integrated once in closed form, the second integration must be carried out numerically. Therefore, the integration was programmed for the CDC 3100 computer at Electro-Optical Systems, Inc. A typical family of η versus ξ computer solutions for a temperature ratio $\alpha = 2.022$ and several values of β is shown in Fig. 4-3. This temperature ratio (α) was selected to match experimental conditions of variable parameter vehicle experiments performed earlier.

Since there is no a priori way to establish the ratio β without knowing the potential distribution, an iterative procedure has to be used to compute a voltage output-versus-spacing curve to compare with experimental data. The procedure has been established and programmed for the computer. Basically, it involves six steps and requires numerical inputs on six parameters obtained from experiment. The experimental parameters are:

a. emitter temperature, T_e
b. collector temperature, T_c
c. emitter work function, ϕ_e
d. collector work function, ϕ_c
e. diode current density, J
f. interelectrode spacing, d

For a given $\alpha = T_e/T_c$, the steps in one iteration are:

a. Select a trial value of the ratio β, say β_1.
b. Using α, T_e, J, and β_1, compute n_{em}. This step utilizes an expression for the diode current density which is derived by summing the current densities from each electrode. The current densities are

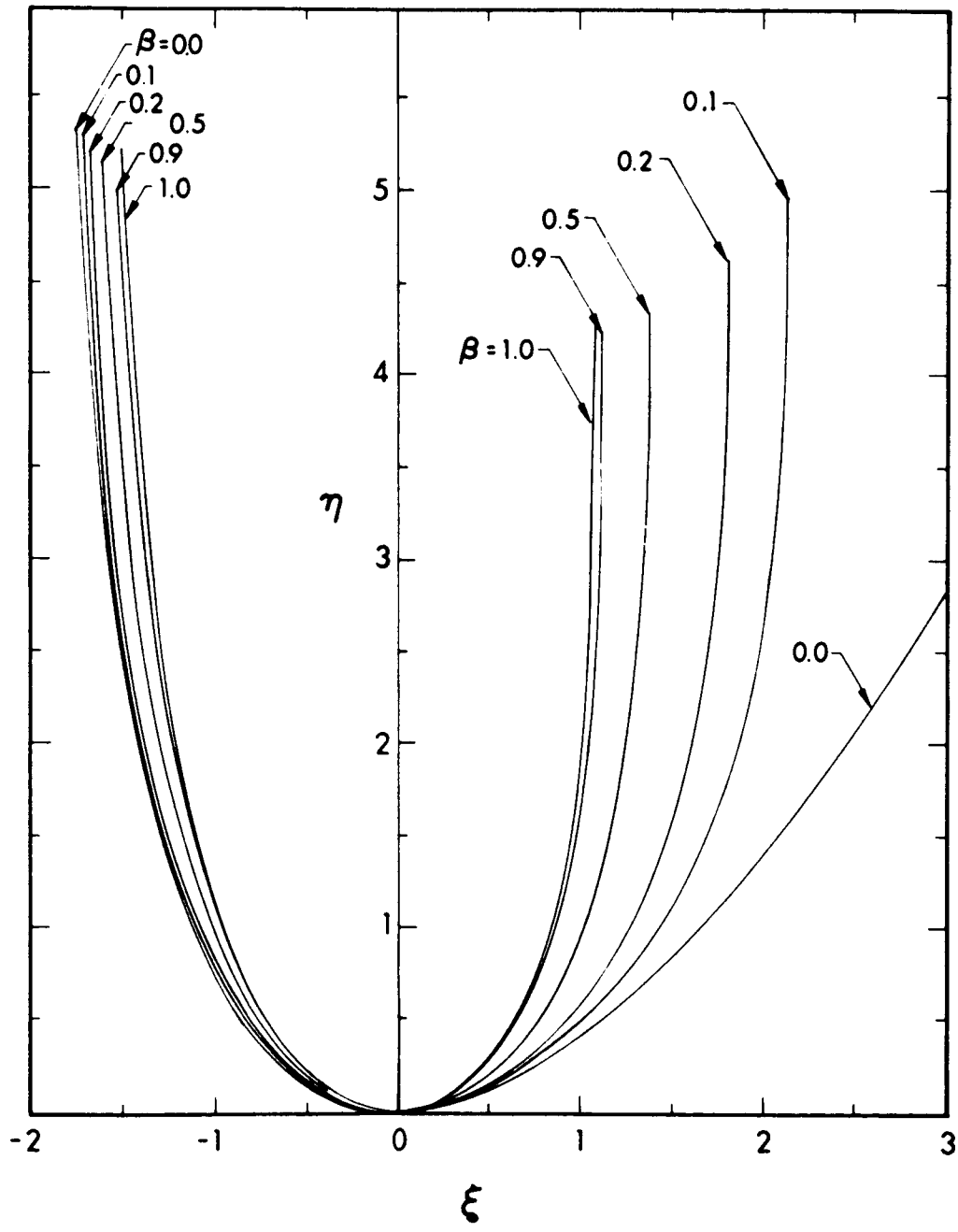

FIG. 4-3 NORMALIZED POTENTIAL DISTRIBUTION (η) VERSUS NORMALIZED COORDINATE (ξ) IN THE INTERELECTRODE SPACE FOR THE CASE OF α = 2.02215 AND SEVERAL VALUES OF β. (α and β are defined in the text)

$$J_e = en_{em}(2kT_e/\pi m)^{1/2}$$

and

$$J_c = -en_{cm}(2kT_c/\pi m)^{1/2}$$

Using the definitions of α and β, the total current density can be written

$$J = e(2kT_e/\pi m)^{1/2} n_{em}(1 - \beta/\alpha^{1/2}) \qquad (22)$$

Thus,

$$n_{em} = J(\pi m/2e^2 kT_e)^{1/2}(1 - \beta/\alpha^{1/2})^{-1} \qquad (23)$$

c. Using a value of n_{eo} computed with Eq. 2 and the value of n_{em} computed with Eq. 23, compute the ratio $n_{eo}/2n_{em}$. This ratio is related through Eq. 9 to the difference in potential (and its equivalent dimensionless η) between the emitter surface and the potential minimum. Consequently, this computation and the curve of Fig. 4-3 for the trial β establishes a point on the abscissa of Fig. 4-3 to the left of the potential minimum. Let this point be denoted by ξ_e.

d. Calculate $n_{cd}/2n_{cm} = n_{cd}/2\beta n_{em}$ by the same procedure used in step c. The equation for n_{cd} is identical to Eq. 9 with φ_c and T_c substituted for φ_e and T_e. This step establishes a second point on the abscissa of Fig. 4-3 to the right of the potential minimum; call this point ξ_c.

e. Using the experimental value of d, compute d/λ using Eq. 20. Call this ratio ξ_d.

f. Compare $\xi_c - \xi_e$ with ξ_d. If $\xi_c - \xi_e > \xi_d$, the trial value of β is too small: that is, the dimensionless interelectrode spacing calculated using β_1 is smaller than the actual dimensionless spacing, d/λ. If $\xi_c - \xi_e < \xi_d$, the trial value of β is too large.

These six steps are repeated until a trial β is found which yields $\xi_c - \xi_e = \xi_d$. This establishes the proper β and the correct potential distribution for the six experimental conditions itemized above. When the proper β is found, the difference between the dimensionless potentials

at the surface of the electrodes is determined. Converting the dimensionless potentials to dimensional form yields the diode electrode surface potential difference, $V = V_a + \varphi_e - \varphi_c$. V_a, the applied or generated output voltage, is obtained by subtracting the contact potential difference, $\varphi_e - \varphi_c$, from V. The net result thus is a calculated output voltage appropriate for the given interelectrode spacing, d.

Prior to setting up the computer program for the interative procedure, each step was carried out with a desk calculator for a specific case. Although the results are preliminary, it appears that there is agreement within experimental error between the computed value of V_a and the experimental value obtained from the variable parameter test vehicle. These results will be discussed in a subsequent report.

REFERENCES

1. A. E. Campbell, Jr., D. H. Pollock, and A. O. Jensen, "Precision Measurements of the Characteristics of a Low-Energy Cesium Vapor Plasma," Proceedings of the Twenty-Sixth Annual Conference on Physical Electronics, pp. 25-39

2. A. E. Campbell, Jr., "High Performance Thermionic Converters," JPL Contract 951225, Final Report

3. A. E. Campbell, Jr. and A. O. Jensen, "Detailed Measurements of the Characteristics of a Low-Energy Cesium Vapor Plasma," Thermionic Specialist Conference, Houston, Texas, Nov. 1966

4. Anthony F. Dugan,"Contribution of Anode Emission to Space Charge in Thermionic Power Converters," J. Appl. Phys. 31, 1397 (1960)